METEOR-Berichte

***Eddy Study to Understand Physical-Chemical-Biological Coupling and the Biological Carbon Pump as a Function of Eddy Type off West Africa***

Cruise No. M160

23.11.2019 – 20.12.2019,
Mindelo (Cabo Verde) – Mindelo (Cabo Verde)
MOSES Eddy Study II

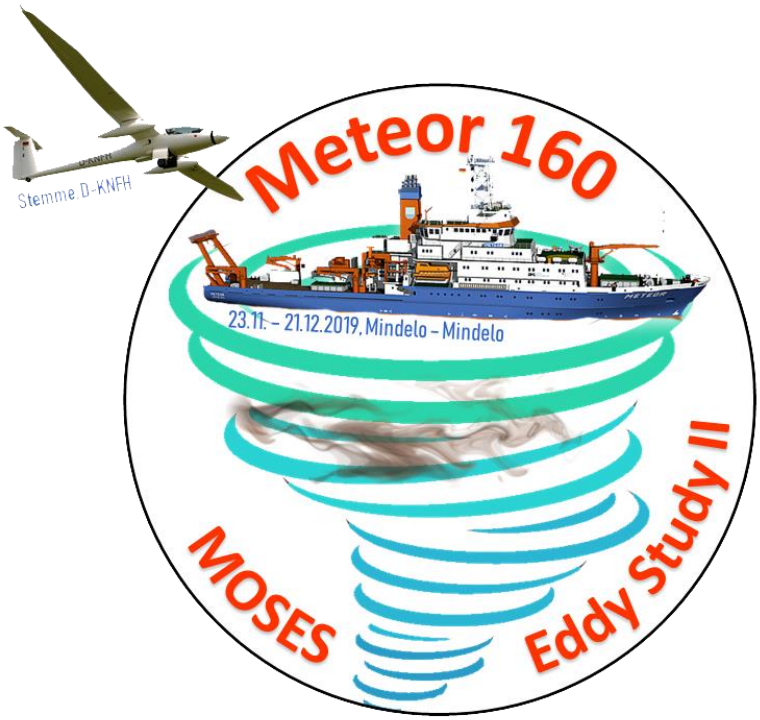


A. Körtzinger, A. Andrae, B. Baschek, K. Becker, D. Behr, D. Blandfort, P. Calil, R. Carrasco, M. Dengler, Q. Devresse, A. Engel, B. Fiedler, G. Fischer, T. Fischer, C. Flintrop, K.W. Fomba, S. Golde, T. Hahn, H. Hauss, H. Hepach, K. Heymann, M. Hieronymi, J. Horstmann, L. Hufnagel, M. Iversen, J. Karstensen, S. Katzenmeier, J. Knudsen, T. Kock, G. Krahmann, H. Krasemann, L. Merckelbach, N. Moradi, M. Nothof, M. Paulsen, A. Raeke, R. Röttgers, L. Schultze, T. Stoeck

Chief Scientist: Arne Körtzinger
GEOMAR Helmholtz Centre for Ocean Research Kiel

2020

**Table of Contents**

# 1 Cruise Summary

## 1.1 Summary in English

Cruise M160 is part of concerted MOSES/REEBUS Eddy Study featuring three major research expeditions (M156, M160, MSM104). It aims to develop both a qualitative and quantitative understanding of the role of physical-chemical-biological coupling in eddies for the biological pump. The study is part of the MOSES "Ocean Eddies" event chain, which follows three major hypotheses to be addressed by the MOSES/REEBUS field campaigns:

(1) Mesoscale and sub-mesoscale eddies play an important role in transferring energy along the energy cascade from the large-scale circulation to dissipation at the molecular level.

(2) Mesoscale and sub-mesoscale eddies are important drivers in determining onset, magnitude and characteristics of biological productivity in the ocean and contribute significantly to global primary production and particle export and transfer to the deep ocean.

(3) Mesoscale and sub-mesoscale eddies are important for shaping extreme biogeochemical environments (e.g., pH, oxygen) in the oceans, thus acting as a source/sink function for greenhouse gases.

In contrast to the other two legs, MOSES Eddy Study II during M160 did not include any benthic work but focused entirely on the pelagic dynamics within eddies. It accomplished a multi-disciplinary, multi-parameter and multi-platform study of two discrete cyclonic eddies in an unprecedented complexity. The pre-cruise search for discrete eddies suitable for detailed study during M160 had already started a few months prior to the cruise. Remote sensing data products (sea surface height, sea surface temperature, ocean color/chlorophyll a) were used in combination with eddy detection algorithms and numerical modelling to identify and track eddies in the entire eddy field off West Africa. In addition, 2 gliders and 1 waveglider had been set out from Mindelo/Cabo Verde for pre-cruise mapping of the potential working area north of the Cabo Verdean archipelago.

At the start of M160, a few suitable eddies – mostly of cyclonic type – had been identified, some of which were outside the safe operation range of the motorglider plane. As technical problems delayed the flight operations, the first eddy (center at 14.5°N/25°W) for detailed study was chosen to the southwest of the island of Fogo. It was decided to carry out a first hydrographic survey there followed by the deployment of a suite of instruments (gliders, waveglider, floats, drifter short-term mooring). Such instrumented, we left this first eddy and transited – via a strong anticyclonic feature southwest of the island of Santiago – to the region northeast of the island of Sal, i.e. in the working range of the glider plane. During the transit, a full suite of underway measurements as well as CTD/RO section along 22°W (16°-18.5°N) were carried in search for sub-surface expressions of anticyclonic eddy features.

In the northeast, we had identified the second strong cyclonic eddy (center at 18°N/22.5°W) which was chosen for detailed study starting with a complete hydrographic survey (ADCP, CTD/RO, other routine station work). After completion of the mesoscale work program, we identified a strong frontal region at the southwestern rim of the cyclonic eddy, which was chosen for the first sub-mesoscale study with aerial observation component. There, the first dye release experiment was carried out which consisted of the dye release itself followed by an intense multi-platforms study of the vertical and horizontal spreading of the initial dye streak. This work was

supported and partly guided by aerial observation of the research motorglider Stemme, which was still somewhat compromised by technical issues and meteorological conditions (high cloud cover, Saharan dust event). Nevertheless, this first dye release experiment was successful and showed rapid movement of the dynamic meandering front.

After completion of work on this second eddy and execution of a focused sampling program at the Cape Verde Ocean Observation, RV METEOR returned to the first eddy for continuation of the work started there in the beginning of the cruise. This was accompanied by a relocation of the airbase of Stemme from the international airport of Sal to the domestic airport of Fogo. The further execution of the eddy study at this first eddy, which again included a complete hydrographic survey followed by a mesoscale eddy study with dye release, was therefore possible with aerial observations providing important guidance for work on RV METEOR.

Overall, M160 accomplished an extremely intense and complex work program with 212 instrument deployments during station work, 137 h of observation with towed instruments and a wide range of underway measurements throughout the cruise. Up to about 30 individually tracked platforms (Seadrones, glider, wavegliders, drifters, floats) were in the water at the same time providing unprecedented and orchestrated observation capabilities in an eddy. All planned work components were achieved and all working groups acquired the expected numbers of instrument deployments and sampling opportunities.

## 1.2 Zusammenfassung

Die Expedition M160 ist Teil der konzertierten MOSES/REEBUS-Wirbelstudie mit drei großen Forschungsexpeditionen (M156, M160, MSM 104), deren Ziel es ist, sowohl ein qualitatives als auch ein quantitatives Verständnis der Rolle der physikalisch-chemisch-biologischen Kopplung in Ozeanwirbeln für die biologische Pumpe zu entwickeln. Die Studie ist Teil der MOSES Ozeanwirbel-Ereigniskette, die drei Haupthypothesen folgt, welche in den MOSES/REEBUS-Feldkampagnen behandelt werden sollen:

(1) Mesoskalige und submesoskalige Wirbel spielen eine wichtige Rolle bei der Energieübertragung entlang der Energiekaskade von der großräumigen Zirkulation zur Dissipation auf molekularer Ebene.

(2) Mesoskalige und submesoskalige Wirbel sind wichtige Faktoren, die Charakteristika der biologischen Produktivität im Ozean bestimmen und wesentlich zur globalen Primärproduktion sowie zum Export und Transfer von Partikeln in die Tiefsee beitragen.

(3) Mesoskalige und submesoskalige Wirbel sind wichtig für die Ausprägung extremer biogeochemischer Umweltfaktoren (z.B. pH-Wert, Sauerstoff) in den Ozeanen und wirken sich somit auf die Quellen/Senken-Funktion für Treibhausgase aus.

Im Gegensatz zu den anderen beiden Expeditionen umfasste die MOSES Eddy Study II während M160 keine benthischen Arbeiten, sondern konzentrierte sich ausschließlich auf die pelagische Dynamik innerhalb von Wirbeln. Sie führte eine multidisziplinäre, multiparametrische und plattformübergreifende Studie von zwei diskreten zyklonalen Wirbeln in einer noch nie dagewesenen Komplexität durch.

Die Suche nach diskreten Wirbeln, die sich für eine detaillierte Untersuchung während M160 eignen, hatte bereits einige Monate vor Beginn der Expedition begonnen. Datenprodukte der Fernerkundung (Meeresspiegelhöhe, Meeresoberflächentemperatur, Ozeanfarbe/Chlorophyll a)

wurden in Kombination mit Wirbeldetektionsalgorithmen und Modellierung zur Identifizierung und Verfolgung von Wirbeln im gesamten Wirbelfeld vor Westafrika verwendet. Darüber hinaus waren 2 Gleiter und 1 Waveglider von Mindelo/Cabo Verde aus zur Voruntersuchung des potentiellen Arbeitsgebietes nördlich des kapverdischen Archipels ausgesetzt worden.

Zu Beginn von M160 waren mehrere geeignete Wirbel – meist zyklonaler Art – identifiziert worden, von denen einige außerhalb des sicheren Arbeitsbereichs des Motorseglerplans lagen. Da technische Probleme den Flugbetrieb verzögerten, wurde als erster ein Wirbel (Zentrum bei 14,5°N/25°W) südwestlich der Insel Fogo für eine detaillierte Untersuchung ausgewählt. Es wurde beschlossen, dort eine erste hydrographische Vermessung durchzuführen, gefolgt vom Einsatz einer Reihe von Instrumenten (Geiter, Waveglider, Drifter, Kurzzeitverankerung). Derartig instrumentiert verließen wir diesen ersten Wirbel und fuhren – über eine starke antizyklonale Struktur südwestlich der Insel Santiago – in die Region nordöstlich der Insel Sal, d.h. in den Arbeitsbereich des Segelflugzeugs. Während des Transits wurde eine ganze Reihe von Unterwegsmessungen sowie ein CTD/RO-Schnitt entlang 22°W (16°-18,5°N) durchgeführt, um nach Strukturen antizyklonaler Wirbel zu suchen.

Im Nordosten hatten wir den zweiten starken zyklonalen Wirbel (Zentrum bei 18°N/22,5°W) identifiziert, der für eine detaillierte Studie ausgewählt wurde, welche mit einer vollständigen hydrographischen Vermessung (ADCP, CTD/RO, andere routinemäßige Stationsarbeiten) begann. Nach Abschluss des mesoskaligen Arbeitsprogramms identifizierten wir eine starke Frontenregion am südwestlichen Rand des Wirbels, die für die erste submesoskalige Studie mit Luftbeobachtungskomponente ausgewählt wurde. Dort wurde das erste Farbstoffexperiment durchgeführt, das aus der Auslegung des Farbstoffs selbst bestand, gefolgt von einer intensiven Multi-Plattform-Studie der vertikalen und horizontalen Ausbreitung des anfänglichen Farbstoffstreifens. Diese Arbeiten wurden durch die Luftbeobachtung mit dem Forschungs-Motorsegler Stemme unterstützt und teilweise geleitet, die jedoch durch technische Probleme und meteorologische Bedingungen (hohe Bewölkung, Staubereignis aus der Sahara) noch etwas beeinträchtigt war. Dennoch war dieses erste Farbstoffexperiment erfolgreich und zeigte eine schnelle Bewegung der dynamischen Mäanderfront.

Nach Abschluss der Arbeiten an diesem zweiten Wirbel und der Durchführung eines gezielten Probenahmeprogramms bei der Beobachtung des Cape Verde Ocean Observatory kehrte FS METEOR zum ersten Wirbel zurück, um die dort gleich nach Start der Expedition begonnenen Arbeiten fortzusetzen. Dies ging mit einer Verlegung der Operationsbasis der Stemme vom internationalen Flughafen Sal zum Inlandsflughafen Fogo einher. Die weitere Durchführung der Wirbelstudie an diesem ersten Wirbel, die wiederum eine vollständige hydrographische Vermessung, gefolgt von einer mesoskaligen Wirbelstudie mit Farbstoffexperiment einschloss, erfolgte daher wieder mit Flugzeugfernerkundung, die erneut wichtige Hinweise für die Arbeiten auf FS METEOR lieferten.

Insgesamt führte M160 ein äußerst intensives und komplexes Arbeitsprogramm mit 212 Instrumenteneinsätzen während der Stationsarbeiten, 137 h Beobachtung mit geschleppten Instrumenten und einer großen Bandbreite an laufenden Unterwegsmessungen während der gesamten Fahrt durch. Dabei waren zeitweilig bis zu 30 individuell verfolgte Plattformen (Seadrones, Gleiter, Wellengleiter, Drifter, Floats) im Wasser und boten beispiellose konzertierte Beobachtungsmöglichkeiten in den Wirbeln. Alle geplanten Arbeitskomponenten wurden erreicht, und alle Arbeitsgruppen erhielten die erwartete Anzahl von Instrumenteneinsätzen und Probenahmen.

# 2 Participants

## 2.1 Principal Investigators

| Name | Institution |
|---|---|
| Körtzinger, Arne, Prof. Dr. | GEOMAR |
| Baschek, Burkard, Prof. Dr. | HZG |

## 2.2 Scientific Party

Ship-based scientific party on research vessel METEOR:

| Name | Discipline | Institution |
|---|---|---|
| Körtzinger, Arne, Prof. Dr. | Chem. Oceanogr. / Chief Scientist | GEOMAR |
| Dengler, Marcus, Dr. | Physical Oceanography | GEOMAR |
| Fischer, Tim, Dr. | Physical Oceanography | GEOMAR |
| Chouksey, Manita, Dr. | Physical Oceanography | UNI HH |
| Müller, Mario | Physical Oceanography | GEOMAR |
| Pinck, Andreas | Physical Oceanography | GEOMAR |
| Andrae, Alexandra | Physical Oceanography | GEOMAR |
| Knudsen, Juri | Physical Oceanography | GEOMAR |
| Fiedler, Björn, Dr. | Chemical Oceanography | GEOMAR |
| Paulsen, Melf | Chemical Oceanography | GEOMAR |
| Hahn, Tobias | Chemical Oceanography | GEOMAR |
| Bogner, Boie | Chemical Oceanography | GEOMAR |
| Leibold, Patrick | Data Science | GEOMAR |
| Hepach, Helmke, Dr. | Biological Oceanography | GEOMAR |
| Becker, Kevin, Dr. | Biological Oceanography | GEOMAR |
| Devresse, Quentin | Biological Oceanography | GEOMAR |
| Golde, Sandra | Biological Oceanography | GEOMAR |
| Katzenmeier, Sven | Marine Ecology | UNI KL |
| Nothof, Maren | Marine Ecology | UNI KL |
| Moradi, Nasrollah, Dr. | Marine Biogeochemistry | MARUM |
| Flintrop, Clara | Marine Biogeochemistry | AWI |
| Hufnagel, Lili | Marine Biogeochemistry | MARUM |
| Rezende Calil, Paulo, Dr. | Physical Oceanography | HZG |
| Merckelbach, Lucas, Dr. | Physical Oceanography | HZG |
| Schultze, Larissa, Dr. | Physical Oceanography | HZG |
| Blandfort, Daniel | Physical Oceanography | HZG |
| Kock, Thomas | Physical Oceanography | HZG |
| Carrasco Alvarez, Ruben | Radar Hydrography | HZG |
| Hieronymi, Martin, Dr. | Remote Sensing | HZG |
| Raeke, Andreas | Meteorology | DWD |

Land-based scientific party around research motorglider STEMME:

| Name | Discipline | Institution |
|---|---|---|
| Baschek, Burkard, Prof. Dr. | Remote Sensing | HZG |
| Röttgers, Rüdiger, Dr. | Remote Sensing | HZG |
| Burmester, Henning | Remote Sensing | HZG |
| Carlson, Dan | Remote Sensing | HZG |
| van Oostende, Marit | Remote Sensing | HZG |

## 2.3 Participating Institutions

| | |
|---|---|
| AWI | Alfred-Wegener-Institut Helmholtz-Zentrum für Polar- und Meeresforschung |
| DWD | Deutscher Wetterdienst |
| GEOMAR | GEOMAR Helmholtz-Zentrum für Ozeanforschung Kiel |
| HZG | Institut für Küstenforschung, Helmholtz-Zentrum Geesthacht |
| MARUM | Zentrum für Marine Umweltwissenschaften, Universität Bremen |
| TROPOS | Leibniz-Institut für Troposphärenforschung, Leipzig |
| UNI HH | Institut für Meereskunde, Universität Hamburg |
| UNI KL | Fachbereich Biologie, Universität Kaiserslautern |

# 3 Research Program

## 3.1 Description of the Work Area

The four major Eastern Boundary Upwelling Systems (EBUS) of the world ocean are driven by spatially varying alongshore winds causing offshore Ekman transport of near-surface waters and the upwelling of cold, nutrient and $CO_2$-rich, and oxygen-deficient waters. The biological productivity driven by the upwelled nutrients is disproportionately high given the size of these regions (~1% of total ocean area) and supports major industrial fisheries and a large fraction of global fish catch (Lachkar and Gruber 2012, and references therein). EBUS are vulnerable to various anthropogenic forcing factors such as ocean warming, ocean acidification, and ocean deoxygenation (Gruber 2011). On top of this, EBUS are expected to experience changes in trade wind intensity and/or location and hence upwelling strength (Bakun et al. 2010). The responses of EBUS to these multiple changes, let alone the synergistic nature of their interactions, are largely unknown. This is particularly true for the role of eddies in EBUS and their importance for the biological carbon pump. Our capacity to predict future responses in EBUS under global change trajectories is therefore extremely limited.

Instabilities generated by velocity shear of the coastal current system and the Ekman circulation favor the generation of eddies in EBUS. By trapping coastal waters of upwelling origin and transporting them offshore, these eddies play an important role in the lateral mixing and transport of physical and biogeochemical properties and thereby modulate biogeochemistry and biological productivity. It has been shown that the three types of eddies (cyclonic, anticyclonic, anticyclonic mode-water) have drastically different, far-reaching effects. In the Canary Current System (CanCS), dramatic effects of eddies on subsurface oxygen concentration leading to severe hypoxia and causing redox-dependent biogeochemical and biological responses (Fiedler et al. 2016, Fischer et al. 2016, Grundle et al. 2017, Hauss et al. 2016, Karstensen et al 2017, Löscher et al. 2015, Schütte et al. 2016) have been discovered in a concerted field study (see 3.3). Systematic analyses of all EBUS using coupled models (Gruber et al. 2011) and applying neural networks to potential drivers of biological productivity (Lachkar and Gruber 2012) reveal the prominent role of eddies in these systems. The interaction of eddies and other drivers, such as wind stress variability, is complex, variable among the different EBUS and insufficiently understood due to a lack of observations connecting the relevant spatial scales.

Eddies, an omnipresent feature of the tropical northeast Atlantic Ocean, are generated off West Africa throughout the year with a peak in frequency during summer. At an average propagation speed of 3.0 ± 2.5 km $d^{-1}$ along their typical westward trajectories this peak in eddy abundance reaches the region to the northeast of the Cabo Verdean archipelago by November/December. The timing of cruise M160 therefore provided the highest likelihood of encountering strong eddies in the working area, the extension of which was to some extent constrained by the safe operation range of the STEMME S10 VTX motorglider (Aachen University of Applied Sciences) used for parallel airborne observations of sub-mesoscale eddy features.

Eddies can be considered as a continuation of the upwelling system transporting material and properties laterally into the open ocean. Specific dynamical processes associated with eddies and their sub-mesoscale features enhance vertical mixing and transport pathways that even lead to upwelling en route. In particular, the role of strong vertical velocities associated with energetic sub-mesoscale fronts at the outer edge of mesoscale eddies may be an important mechanism for

nutrient input into the surface layer. Evidence exists that these areas of very intense cross-diapycnal flux are close in space to areas of low mixing. The governing dynamical processes are largely unknown and so is the overall biogeochemical and ecosystem response. Eddies are important factors determining the quantity of biological production as well as the fate of upwelled nutrients and fixed organic carbon and thereby the overall $CO_2$ source/sink function of EBUS. Intensification of trade winds and surface currents will impact coastal upwelling systems directly through changes in upwelling intensity and possibly also indirectly through changing eddy activity. Due to the counteractive effects of upwelling intensity on the one hand and eddy activity, mixed layer depths and continental shelf width on the other hand, these changes are likely to play out differently in all four EBUS and warrant dedicated studies of the overall responses of EBUS. Cruise M160 is part of a concerted field study focusing on the role of eddies in the CanCS aimed at understanding their role in the physical, chemical, and biological dynamics for the region.

### 3.2 Aims of the Cruise

With the concerted MOSES Eddy Study featuring three major research expeditions (M156, M160, 3rd cruise in 2021) we aim to develop both a qualitative and quantitative understanding of the role of physical-chemical-biological coupling in eddies for the biological pump. The study is part of the MOSES "Ocean Eddies" event chain, which follows three major hypotheses to be addressed by MOSES field campaigns:

(4) Mesoscale and sub-mesoscale eddies play an important role in transferring energy along the energy cascade from the large-scale circulation to dissipation at the molecular level.

(5) Mesoscale and sub-mesoscale eddies are important drivers in determining onset, magnitude and characteristics of biological productivity in the ocean and contribute significantly to global primary production and particle export and transfer to the deep ocean.

(6) Mesoscale and sub-mesoscale eddies are important for shaping extreme biogeochemical environments (e.g., pH, oxygen) in the oceans, thus acting as a source/sink function for greenhouse gases.

The ultimate goal of cruise M160 (MOSES Eddy Study II) was to contribute significantly to our understanding of how ocean eddies generated in one of the major eastern boundary upwelling systems, i.e. the Canary Current system, shape and mediate ocean productivity and vertical carbon export via the biological carbon pump. For this purpose, we planned to carry out a detailed high-resolution, multi-parameter, interdisciplinary study of two individual eddies in Cabo Verdean waters.

### 3.3 Agenda of the Cruise

Cruise M160 was the second in a series of three cruise legs forming a dedicated multi- and interdisciplinary eddy study (MOSES Eddy Study I–III) which employs the 'Modular Observation Solutions for Earth Systems' (MOSES) infrastructure of the Helmholtz Association (HGF). MOSES is a novel observing system developed by the centers in the HGF Research Field Earth and Environment (moses.eskp.de/home). It comprises highly flexible and mobile observation modules, which are designed to investigate the interactions of short-term events and long-term trends across Earth compartments. MOSES conceptually follows an event chain approach. The 3-leg study is the first major field campaign of the MOSES Ocean Eddies event chain. It started with M156 and will end with cruise MSM104 to be lead by Prof. Jens Greinert from GEOMAR. The

main goal of M160, the second of the three expeditions, was to carry out both detailed mesoscale and sub-mesoscale studies of two individual eddies selected through an early detection, tracking and verification scheme based on remote sensing and in-situ information from autonomous platforms collected prior to the cruise.

This ambitious eddy study built on an interdisciplinary approach demonstrated successfully during the 2014 "Eddy Hunt Project" (GEOMAR & Kiel University; Fiedler et al. 2016, Fischer et al. 2016, Grundle et al. 2017, Hauss et al. 2016, Karstensen et al 2017, Löscher et al. 2015, Schütte et al. 2016) combined with the successful approaches of the sub-mesoscale studies SubEx I & II and the "Expedition Clockwork Ocean" (HZG). Using refined automated detection methods employing remote sensing products (sea level anomaly, sea surface temperature, ocean color) early detection of eddies was possible during the months preceding the cruise. For groundtruthing of potential candidate eddies, 2 ocean gliders and 1 wave glider were deployed from the 'Ocean Science Centre Mindelo' (www.oscm.cv) prior to the cruise.

The general concept of the eddy study started with a detailed survey of mesoscale properties of an eddy. This included the current field in the upper 1200 m as well as physical and a whole suite of biogeochemical and biological properties at the surface and in the upper 1200 m of the water column. On the basis of this survey and with the aid of remote sensing information of temperature, currents and ocean color information – both from satellites and the research glider plane – the exact locations of the sub-mesoscale studies were determined. Both mesoscale and sub-mesoscale studies featured a large range of observational techniques that were deployed in a concerted way. Special attention was given to the frontal region at the boundary of the eddies where strong vertical and horizontal sub-mesoscale motion is concentrated in sharp fronts at the surface connecting matter exchange with the surface layer and across the eddy boundary. Elucidating these contrasting roles by connecting the large range of relevant scales was a major and novel aim of the study.

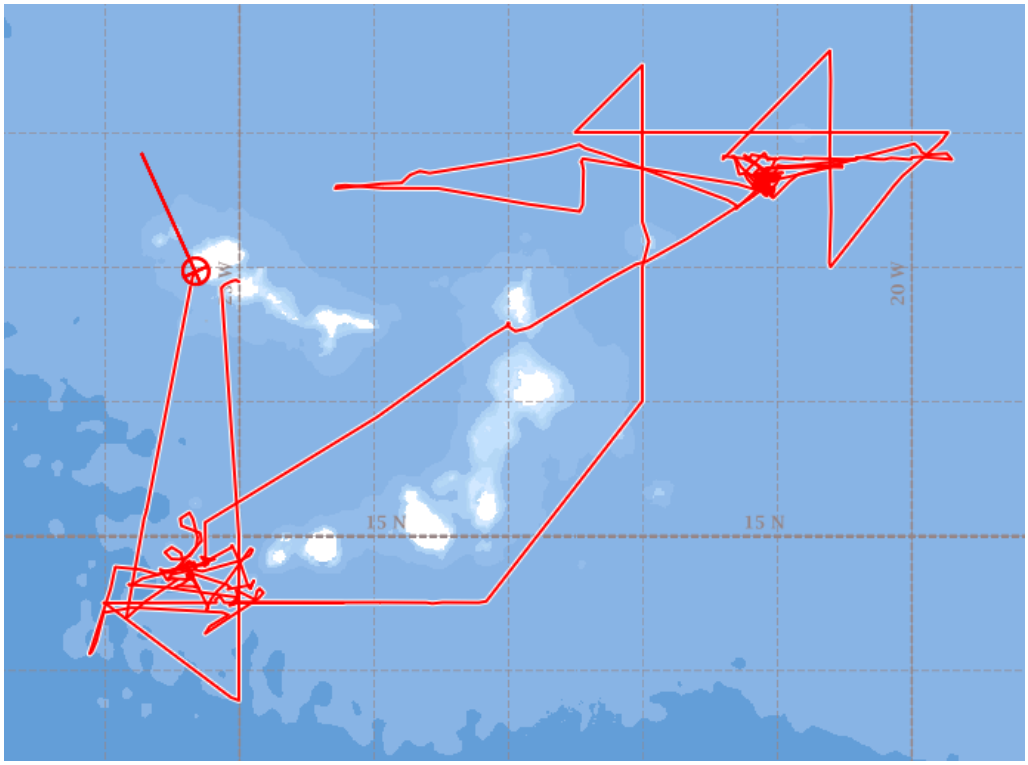


**Fig. 3.1** Track chart of R/V METEOR Cruise M160.

## 4 Narrative of the Cruise

The scientific party of RV METEOR cruise M160 arrived at Mindelo/Cabo Verde between 19/11 and 21/11/2019 and immediately started unpacking and installing the large amount of equipment such that everything had been installed in a seaworthy manner at departure on 23/11/2019. Prior to that, a brief meeting was held on METEOR with the chief pilot and principal investigator of the joint research glider airplane mission and representatives of the Coast Guard of Cabo Verde to discuss aircraft operations, communications and safety issues.

After departure, we headed to the southwest of the islands of Fogo and Brava where satellite imagery suggested the presence of a strong cyclonic eddy. This eddy was surveyed in its entirety along a cross-like pattern with underway current (ADCP) and underway CTD hydrographic measurements. In addition, 1 wave glider, 2 gliders, 2 Argo floats (1 BGC-Argo float) and a surface drifter were deployed around and within the eddy. We furthermore carried out a zonal section across the eddy with the towed instrument array (TIA) of the HZG and deployed a short-term mooring near the eastern flank of the eddy. Finally, a full station program with CTD-rosette, multi opening/closing net and marine snow catcher was performed in the eddy center where also the first 24 h drift experiment with the sediment traps took place. The duration of the 24 h station allowed us to also briefly survey a strong but shallow anticyclonic eddy on the leeward side of the island of Santiago where 2 gliders, 1 float and 1 surface drifter were deployed before return to the cyclone. By this, we aimed at capturing the eddy in its current state as reference to the situation when returning to it for detailed study towards the end of the cruise.

After completion of this eddy pre-survey, we departed on 26/11/2019 for a new study area to the northeast of the Cabo Verdean archipelago, where interesting eddy features had shown up in the satellite images. On the way, we performed a CTD/ADCP section to 1200 m depth along 22°W reaching to 18.5°N (28/11/2019) where we carried out a search for a possible anticyclonic modewater eddy (ACME) which express themselves only very weakly in satellite data. In situ data from the gliders and wave glider, however, had given us – already prior to the start of the M160 cruise – some hints of the presence of such a feature in that region. The survey revealed indeed shallow filaments of strongly oxygen-depleted water, which could be remnants of an ACME, but no coherent eddy.

We therefore decided to head east towards a large and dynamic cyclonic eddy centered around 18°N/22°36'W where we spent the next 12 days (29/11 to 10/12/2019) and executed the first complete eddy study program starting with a detailed ADCP and CTD/RO survey along a cross-like pattern spanning the entire eddy into surrounding waters. During the course of this, 5 gliders, 3 floats (2 BGC-Argo floats) and surface drifters were deployed. One of our wave gliders was recovered, refurbished and re-deployed. Also, two 24 h sediment trap drifters with biogeochemical sensor package in the mixed layer were deployed in different locations of the eddy (center, rim).

This eddy was chosen also for the first detailed study of sub-mesoscale eddy dynamics. After a larger ADCP, X-band radar and thermosalinograph survey in the southwestern frontal region, a target area was identified where a clear thermal front was located. In a distance of about 1 nm on the cold eddy-side of the front, the first of two dye release experiments was carried out. For this experiment, about 70 kg of the non-toxic, environmentally harmless water tracer rhodamine WT were prepared in about 900 L of a water-isopropanol solution, the density of which was carefully adjusted to the target density at planned deployment depth. For deployment, a hose was lowered attached to a modified CTD with rhodamine sensor to the target depth of about 65 m. By means

of a pump, the dye solution was then pumped at constant rate down to the end of the hose where it was dispersed through a 1 m long holey pipe into the waters. We adjusted the ship speed through water to about 1 knot while a pump rate of approx. 1000 L $h^{-1}$ was maintained. This way, the dye was laid out as narrow and thin streak with a length of nearly 1 nm. Right after deployment, the TIA was towed across the dye streak in a zigzag pattern allowing us to map the depth-density-temperature range and the geographical location to which the streak had actually been placed. In the following 3 days, we repeatedly returned to the dye streak to map its changing location and shape. After the initial spreading, we changed from the TIA to the Moving Vessel Profiler (MVP), a free falling CTD sensor package with rhodamine sensor and its own winch that allows CTD profiles to be taken of the upper 100 m at about 4-5 min separation from the moving vessel. While this method gave less horizontal resolution, it provided beautifully resolved peaks of the vertical dye distribution.

As complementary observational component of the sub-mesoscale eddy study, the research motorglider STEMME of the University of Applied Sciences in Aachen was used for aerial observations of temperature (infrared camera) and ocean color/chlorophyll (hyperspectral camera) by the HZG Institute for Coastal Research. Initial technical problems with the aircraft and the scientific payload delayed the start of the aircraft operations. Strongly overcast cloud conditions and the long distance between study area and the plane's base at Sal airport further reduced the time window for aerial observations. Nevertheless, a few successful flights with nice IR images of the frontal situation in the sub-mesoscale study area could be achieved from a flight altitude of about 5000 m.

Towards the end of the work program at this cyclonic eddy, unfavorable weather conditions with wind force around 7 Bft prevented the planned, zodiac-based recovery of 6 gliders and 1 wave glider. In order to save ship time while waiting for somewhat calmer conditions, we preponed the visit to the long-term time series station "Cape Verde Ocean Observatory" (CVOO). Station work there included among standard instruments a further float and surface drifter deployment. After completion of the CVOO station (08/12 – 10/12/2019), we returned to the eddy where conditions had only slightly improved but still prevented deployment of the zodiac for glider recoveries. We therefore decided to use the "Rescue Star" for recoveries, an instrument developed specifically for the rescue of shipwrecked people during bad weather conditions and heavy sea state. Using this device, we were able to safely recover all 6 gliders, 5 of which had previously been aligned into a straight formation with close distances of 0.5-1 nm at the sea surface so that they could all be recovered in record-breaking 2 h in total.

After the work at this eddy was finished, we returned to the cyclone southwest of Fogo Island which had remained very intense throughout this cruise. Due to time constraints, we repeated the full eddy study program of the first eddy here but for large parts in parallel (11/12 – 18/12/2019). Again, underway ADCP, X-band radar and thermosalinograph survey were combined with the full station work including 3 additional 24 h drift stations, glider, wave glider, float and surface drifter deployments etc. Operations went very smoothly although the parallel execution of the mesoscale and sub-mesoscale surveys and the synchronization with the flight operations placed several additional time constraints on the work plan and made planning rather complex. For the sub-mesoscale component, the dye release experiment was repeated successfully in a very similar way, this time near the eddy center at about 45 m depth. There, very cold water (up to 5°C temperature

contrast to surrounding non-eddy waters) with clear upwelling signatures and drastically elevated primary and secondary production had been encountered.

The aircraft team had decided to move operations from the international airport of Sal to the small domestic airport of Fogo. The resulting proximity to the Fogo eddy allowed longer observation times at lower altitude (about 3000 m) yielding more and better data. During the sub-mesoscale studies, some beautiful infrared and hyperspectral image maps of staggered thermal fronts around the eddy core were obtained and allowed the METEOR to perform its TIA and X-band radar observations as well as its hyperspectral light measurements to be guided by and synchronized with the aircraft. These studies again showed highly dynamic features even near the eddy center pointing at rapid adjustment processes possibly triggered by a drop in the prevailing wind forcing. The final flight finished with a close overflight of RV METEOR on 15/12/2019. The aircraft and the entire team then flew back to Sal to dismantle the plane and stow it into a 40'-container for shipment back to Aachen.

The METEOR continued the Fogo eddy study until 19/11/2019. During that time we started the recovery of the manifold instruments that we had placed in the eddy. The short-term mooring as well as the 2 wave gliders were successfully recovered on 16/12/2019 while the gliders stayed active until 18/12/2019. The final CTD cast was performed late on 17/12/2019 allowing groups to wind down operations already on 18/12/2019. The short transit to Mindelo prevented all groups from relaxing after the end of the work program, as all equipment had to be dismantled, cleaned, packed and prepared for shipment prior until the evening of 20/12/2019. On 19/12/2019, RV METEOR and RV MARIA S. MERIAN had a brief rendezvous at sea – in the sheltered bay of Tarrafal on the Cabo Verdean island of Santo Antão. The cruise ended after 3845 nautical miles in the morning of 20/12/2019 in Mindelo.

Throughout the cruise, meetings with the captain and the heads of the ship departments were held every day at 8:00 board time. In addition, we had a full science meeting with discussion of work progress, first results, following work plan as well as status of instruments everyday at 10:00 board time. Finally, a brief teleconference was held nearly every day at 19:30 board time with the airplane team for discussion of previous and upcoming flight missions and their synchronization with the ship operations.

Given the complexity and density of the work program, the parallel execution of different yet connected studies (mesoscale, sub-mesoscale, aerial) and the very large number of instruments operated both on board and autonomously in the ocean it is amazing how smooth, cooperative and successful it could be carried through to the end. All cruise objectives were met and all groups received very much all their requested station time and sample material.

# 5 Preliminary Results

## 5.1 Physical Oceanography

### 5.1.1 Hydrographic Survey (CTD/RO, uCTD, MVP)

(M. Dengler[1], J. Knudsen[1], T. Fischer[1], G. Krahmann[1])
[1]GEOMAR

#### 5.1.1.1 CTD-Rosette System

During M160, a total of 73 vertical profiles of pressure (P), temperature (T), conductivity (C) and oxygen (O) were recorded. Most CTD/$O_2$ profiles ranged from the surface to 1200 m depth and only two full depth profiles were taken. We used a Seabird Electronics (SBE) 9plus system, attached to the water sampler carousel, and recent SBE Seasave software. The SBE underwater unit had, in addition to its own pressure sensor, two parallel sensor sets for T, C, and O. Many additional sensors were attached to the CTD frame: A Wetlabs turbidity/chlorophyll sensor, a fluorescence sensor (SN 2294), a Wetlabs CDOM sensor (SN 2377), and a photosynthetically active radiation sensor (PAR, SN 70714). Furthermore, an underwater vision profiler (UVP), a continuous particle imaging classification system (CPICS) and an UV spectral sensor for the measurement of nitrate (OPUS) were mounted on the CTD frame. A Valeport altimeter system (SN 42299) was used during the cruise for bottom distance detection of the CTD. The CTD system itself performed without major problems throughout the whole cruise.

The serial numbers of the primary sensors (1) and secondary sensors (2) were 2463 (T1), 2120 (T2), 2443 (C1), 3959 (C2), 1149(P), 1312 (O1) and 1739 (O2). Occasional spikes were present in the data that were removed by hand editing. On 07/12/2019, just before CTD profile 50, the CTD deck unit 4 malfunctioned and was replaced by deck unit 6, which was used to record CTD data during the rest of the cruise.

#### 5.1.1.2 CTD-Conductivity Sensor Calibration

The calibration of the conductivity and oxygen sensors was conducted following the recommendations in the GO-SHIP manual (www.go-ship.org). For the calibration of the conductivity sensors, we measured 145 water samples with a high-precision salinometer. The conductivity calibration using linear correction terms in P, T, and C resulted in a root mean square (rms) salinity misfit of 0.0025 for the both conductivity sensors after removal of the most deviating 33% of samples. For the final data, the primary string of sensors was selected.

The high-precision salinometer in use was the GEOMAR OPTIMARE Precision Salinometer (OPS 20). Before measuring the conductivity of the water samples with the OPS, the bottled water samples had to be degassed to remove gas micro-bubbles, which would deteriorate the OPS instrument performance. Degassing was done after adjusting the bottles to the lab temperature for about 10 h, then warming the sample bottles in a water bath at a temperature of about 40°C. After approximately 30 min the glass bottles were opened for 1 to 2 s. Then the sample bottles were brought to the salinity lab where their conductivity could be measured after cooling down to the lab temperature for at least 10 h. In the last 3 days of the cruise, the standardization of the instrument did not reach stable values. Conductivity values from the water samples of the last 7

CTD stations could thus not be determined. The reason for the malfunctioning of the OPS 20 could not be determined.

#### 5.1.1.3 Oxygen Sensor Calibration

The calibration of the conductivity and oxygen sensors was conducted following the recommendations in the GO-SHIP manual (www.go-ship.org). For the calibration of the oxygen sensors, 709 measurements of the dissolved oxygen content from water samples using the Winkler titration method were used (see subsection 5.2.1 discrete seawater sampling). The oxygen calibration using linear correction terms in T and O, quadratic correction terms in P as well as the product of P and O resulted in a rms oxygen misfit of 0.58 µmol $kg^{-1}$ and 0.57 µmol $kg^{-1}$ for the two oxygen sensors, respectively.

#### 5.1.1.4 Moving Vessel Profiler

The Moving Vessel Profiler (MVP) was used for underway profiling of upper ocean temperature, salinity, depth, chlorophyll and rhodamine. The system, a MVP30-350 manufactured by AML Oceanographic, consisted of a winch with 440 m of 4-conductor tow cable, a winch frame with an outrigger and an attached sheave, and a tow fish (Fig. 5.1.1.4). The measuring system had just been purchased prior to the cruise and was used on R/V METEOR for the first time. An AML technician helped setting up the measuring system while the vessel was in port in Mindelo prior to the cruise. The MVP was installed on the rear port side of the working deck (Fig. 5.1.1.4) and the MVP controller and laptop were set up in the pulser station (laboratory 11). The controller was receiving NMEA position, depth sounding, and ship speed data from R/V METEOR's central data acquisition unit. We note that due to installation of the MVP on port side, the vessel had to refrain from making starboard turns while the MVP was in use.

**Figure 5.1.1.4:** Elements of the moving vessel profiler system with winch and control box (left), tow fish (middle) and winch frame, outrigger and sheave (right).

The towed fish carried an AML Micro CTD package (SN 9068) composed of a conductivity, temperature and pressure Xchange sensors as well as (most of the time) a Turner C-Fluor fluorometer to measure concentrations of rhodamine dye (see section 5.1.11). In the beginning, a chlorophyll sensor was installed in place of the rhodamine sensor. One advantage of the MVP system is that the profiling data are continuously visualized and recorded on a laptop on board the research vessel while the system is in use. The nominal operating depth of the MVP depends on the vessel speed. We used different choices of profiling depth and vessel speed depending on the desired profile repletion rate and maximum profiling depth. Table 5.1.1 illustrates different choices of the parameters used during the cruise. During the cruise, the MVP was mainly used to sample

the rhodamine dye patches (see section 5.1.11). Altogether, 575 vertical profiles of upper-ocean temperature, salinity and rhodamine were collected. Post-processing of the temperature and salinity data is currently being carried out. Results on the sensor performance and uncertainties will be available in the near future.

**Table 5.1.1.4**: Different settings of MVP profiling depth, vessel speed and underway CTD cast duration used during the cruise.

| Ship speed (kn) | Profiling depth (m) | Tow cable out (m) | Cast duration (mm:ss) |
|---|---|---|---|
| 5 | 80 | 160 - 180 | 03:00 |
| 5.5 | 90 | 200-230 | 04:15 |
| 7 | 90 | 230-260 | 04:40 |
| 7.5 | 90 | 250-290 | 05:00 |

#### 5.1.1.5 Underway CTD Measurements

Apart from the MVP, a second underway CTD profiling system was used during the cruise. The Teledyne Oceanscience Underway-CTD (uCTD) is a compact ship-based system for the measurement of conductivity and temperature profiles while the vessel is underway. It consists of a probe, winch, rewinder, davit and a power supply. During uCTD sampling, the probe internally records pressure, temperature and conductivity data. After the probe is retrieved, the data are transferred to a laptop using the wireless transfer technology Bluetooth.

The uCTD system was installed at starboard stern. A total of 62 underway conductivity-temperature-depth (uCTD) profiles were collected using the uCTD probe (SN 155). All profiles reached depths larger than 300 m while they were taken when the vessel was at full speed (10-11 kn). For the calibration of the sensors, the probes were attached to the CTD/RO for two calibration casts (profiles 26 and 62). The subsequent calibration of temperature and salinity included a thermal lag correction and a temporal drift analysis from the comparison between the CTD-calibrated thermosalinograph data and the uCTD surface measurements.

### 5.1.2 Towed Instrument Array Deployments (TIA)

(P. Calil[1], T. Kock[1], D. Blandfort[1], B. Baschek[1])

[1]HZG

The towed instrument array (TIA) used in M160 consists of a custom-made cable of 450 m at the end of which a depressor is attached. Along the cable, a series of probes with temperature, salinity and either oxygen or chlorophyll/rhodamine fluorescence sensors are placed. During deployment, the ship moves at a slow speed and the cable is paid out by the winch, stopping for attachment of the individual sensors which are clamped onto the cable. Once all sensors are placed in the cable, the ship speed was increased to about 5.5 kn and towing the chain through the water. The sensors perform measurements providing very high resolution hydrographic measurements of the surface ocean. A subset of the data is transmitted via inductive modems into the tow chain and on to the deck station for online visualization, which is essential for decision-making on adaptive sampling.

The first deployment of the TIA in M160 occurred on 26/11/2019, when we did a zonal transect across an anticyclonic spiral/eddy southeast of Fogo. There were a total of 11 deployments of the TIA across specific targets during M160. On two occasions, there were concomitant flights of the STEMME gliderplane, which guided us on targeting specific frontal features. One such example

occurred during deployment 9 (Fig. 5.1.2), where we crossed a cold surface filament of approx. 5 km width.

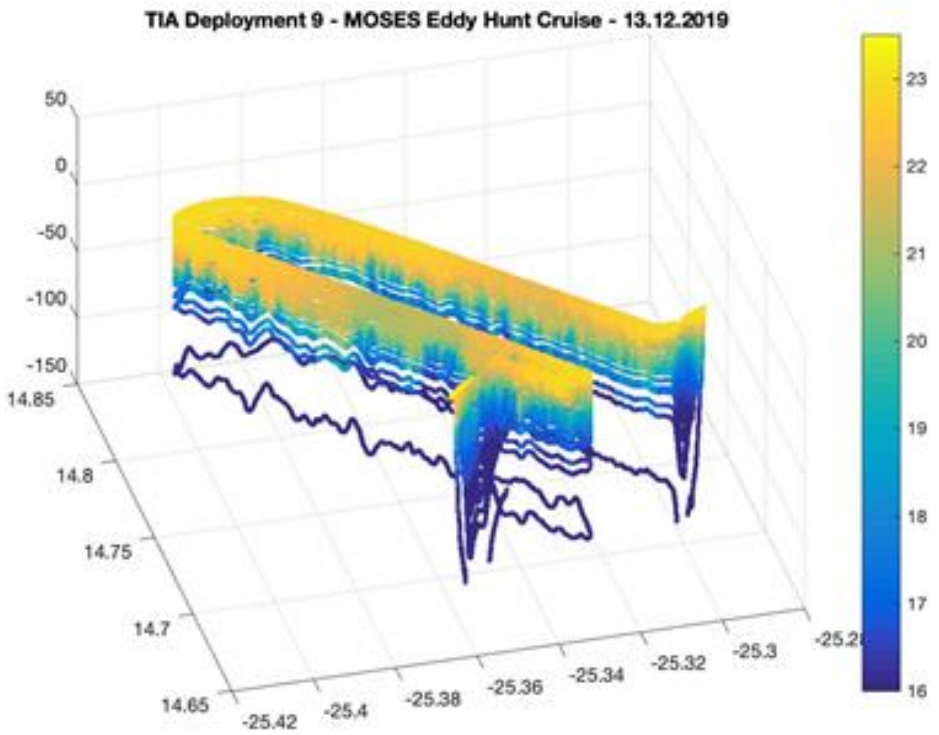


**Figure 5.1.2:** 3D visualization of temperature measurements performed by the TIA system during its 9th deployment on 13/12/2019 of METEOR cruise M160.

In addition to sampling surface fronts, the TIA was also equipped with 3 rhodamine probes, which helped detect the tracer during the dye release experiments. Two such experiments were conducted in which the 3 probes were used in order to provide the spatial distribution of the tracer.

### 5.1.3 Turbulence Measurements (MSS)

(T. Fischer[1], M. Dengler[1])

[1]GEOMAR

A loosely tethered microstructure profiler (MSS 90D, Sea&Sun Technology, SN 73) was used for estimates of turbulent dissipation profiles down to 200 m depth. These will allow estimates of diapycnal mixing and subsequent fluxes of dissolved substances, particularly nutrients. In total, 30 successful MSS stations with 3 consecutive MSS profiles each were performed. The MSS stations immediately followed (in one case immediately preceded) CTD/RO profiles at the same position. The MSS profiler was equipped with 3 airfoil shear sensors (she1: SN 097, she2: SN 135, she3: SN 133), a fast thermistor (SN 081), and common CTD sensors. All sensors worked well throughout the cruise. SN 097 was a bit noisier than the other two shear sensors, but not deteriorating. The onboard-system consisted of winch SN 020, winch motor control SN 3, and deck unit SN 19. The data acquisition software SST_SSDA_226 was configured with files MSS073_2019.spj and MSS073_2019.prb. At station M160_133-1 on 12/12/2019, the profiler delivered no data, so the station was cancelled. The reason for this was a wet winch connector, which could be repaired before the following station.

### 5.1.4 Underway Hydrographic Measurements (TSG)

(M. Dengler[1], J. Knudsen[1], T. Fischer[1], G. Krahmann[1])

[1]GEOMAR

The SBE21 thermosalinographs (TSG) permanently installed on RV METEOR continuously sampled sea surface temperature (SST) and salinity (SSS). The seawater intakes at the vessel's hull are located at 5 m depth on portside (TSG-1, SN 3313) and starboard side bow (TSG-2, SN 3394). Two external sensors (SBE38, port: SN 0747, starboard: SN 0749) measure temperature at the intakes, while the TSG are situated further inside the vessel.

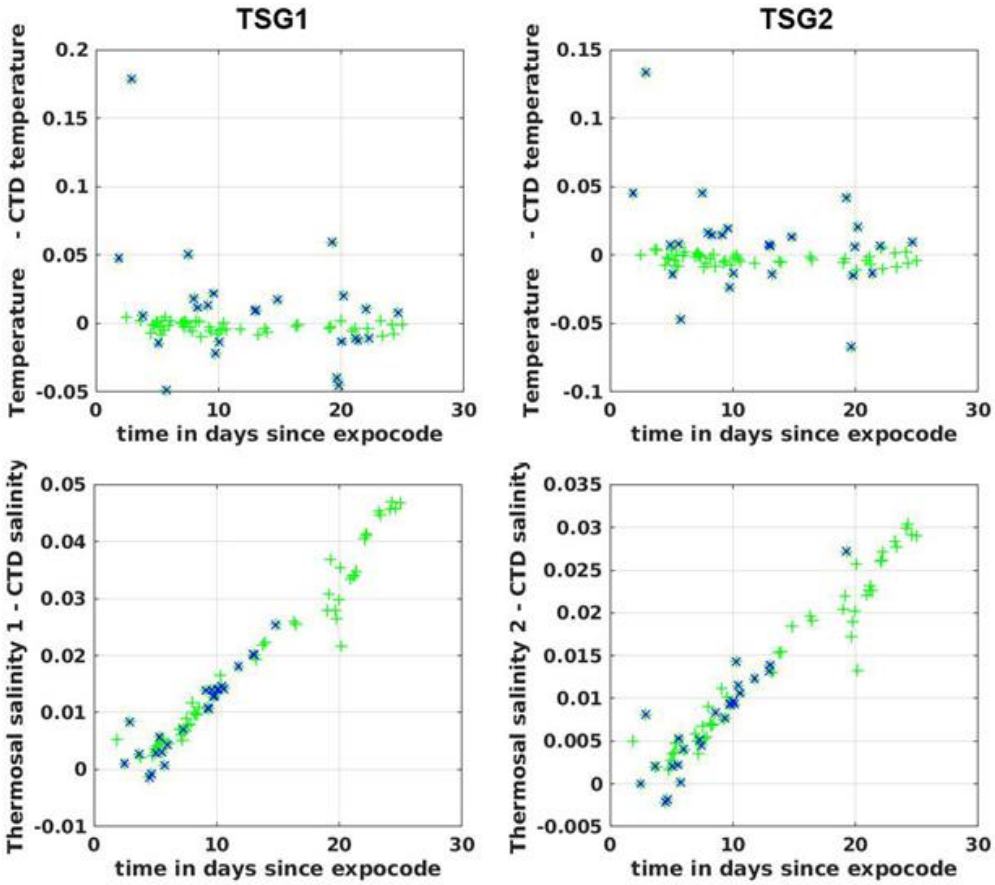


**Figure 5.1.4:** External temperature differences (upper panels) and salinity differences (lower panels) between 5 m CTD and thermosalinograph measurements for TSG1 (left panels) and TSG2 (right panels) vs. time in days since 23/11/2019. Green data points indicate data used for TSG calibration, while data points marked in blue were discarded.

Both TSG performed well throughout the cruise. A comparison of the 5 m temperatures from the CTD and the TSG temperature sensors readings show very good agreement (Fig. 5.1.4). During post-processing, constant offsets of the external TSG temperatures of -0.0023°C (TSG1) and 0.0029°C (TSG2) were corrected. The remaining uncertainty of the TSG temperature readings is 0.004°C for both sensors. TSG-CTD salinity differences linearly increased with time (Fig.5.1.4). Thus, during post-processing a linear temporal trend was removed from the TSG salinity data. After calibration, the uncertainty of the salinity data was 0.0011 for TSG1 and 0.0007 for TSG2 salinity values.

### 5.1.5 Underway Current Measurements (vmADCP)

(T. Fischer[1], A. Andrae[1], M. Dengler[1])

[1]GEOMAR

Two vessel-mounted ADCP systems recorded current velocity profiles. Besides information on the larger flow field, these will provide estimates of the internal wave field. The 75 kHz RDI Ocean Surveyor is hull-mounted and worked throughout the entire cruise from 23/11/2019, 12:13 UTC to 19/12/2019, 12:11 UTC. It was configured to broadband mode with 8 m bins until 12/12/2019 and 5 m bins from 13/12/2019. The transducer misalignment was pre-set to 46° (EA46 in VmDAS software options), so that the misalignment bias of the preprocessed velocities was better than 1 cm $s^{-1}$, i.e. even during cruising at 12 kn the current velocity and direction could be immediately read from the screen. Post-processing showed that an additional 0.07° misalignment angle and an amplitude factor of 1.0033 were needed for an optimal correction. The instrument range was 500 m to 600 m, as usual for broadband mode in the tropics. There had been reports of a defective beam before, however we could not detect missing data, issues or increased error, neither during operation nor during post-processing. However, beam 2 seemed a bit weaker than the other three, and the VmDAS software froze 5 times during the cruise when restarting the system, resulting in some minutes loss of data.

The 38 kHz RDI Ocean Surveyor transducer was placed in the moon pool from 23/11/2019, 12:18 UTC to 03/12/2019, 14:06 UTC (after that it was replaced by a high-frequency ADCP of the TIA group). It was configured to narrowband mode at 32 m bins throughout and reached a range of 1200 m depth. The transducer was very precisely aligned with beam 3 in bow direction (EA0 in VmDAS software options), as the post-processing resulted in a small 0.045° misalignment angle (and amplitude factor 1.0022) for optimal correction.

### 5.1.6 Underway X-Band RADAR Measurements

(R. Carrasco[1], J. Horstmann[1])

[1]HZG

The X-band marine RADAR acquired data in continuous operation mode from 23/11/2019 to 18/12/2019. The 12-kW radar, operating at X-band (9.4 GHz) with vertical polarization in transmit and receive (VV-pol) performed azimuthal scans of the ocean surface at a rotation speed of 20 rotations per minute and was operated as a coherent-on-receive radar system. This means that the random and uncorrelated phases of the radar pulses were recorded and taken into account within the post processing to retrieve the complex backscattered signal from the sea surface. The pulse repetition frequency of the radar was set to 2 kHz, which allows to measure a maximum radial Doppler speed of ±16 m/s without aliasing. The radar was operated with a pulse-length of 50 ns, which resulted in a range resolution of 7.5 m. The antenna had a vertical beam opening of 21° and a width of 7.5 feet (2.3 m) resulting in an azimuthal resolution of ∼1°. The maximum range recorded was 3262.5 m. Around 750,000 RADAR images were acquired during the M160 cruise (7.2 Terabytes).

The RADAR data were processed in real time by the Surface Feature Monitoring System (SuFMoS) which removes the wave, wind and range dependency, integrating all the information in the 2D spatial domain, generating relative surface roughness 2D maps (Fig. 5.1.6.1). The 2D surface roughness maps were utilized to observe ocean surface features, such as signatures of

internal waves (Fig. 5.1.6.1 right), current shear, surface slicks and fronts, in space and time (Fig. 5.1.6.1 left). Furthermore, these images can be utilized to retrieve surface current fields with a resolution of approximately 500 m (Fig. 5.1.6.2). Therefore, the radar image sequences are analyzed with respect to surface wave properties such as wavelength and phase velocity, where the surface current vector results from the difference of the observed phase velocity to that given by the linear dispersion relation of surface gravity waves. All of the post processing of this extensive radar data set will be undertaken by HZG with particular focus on the observation of internal waves, fronts and current shears observed during the TIA deployments.

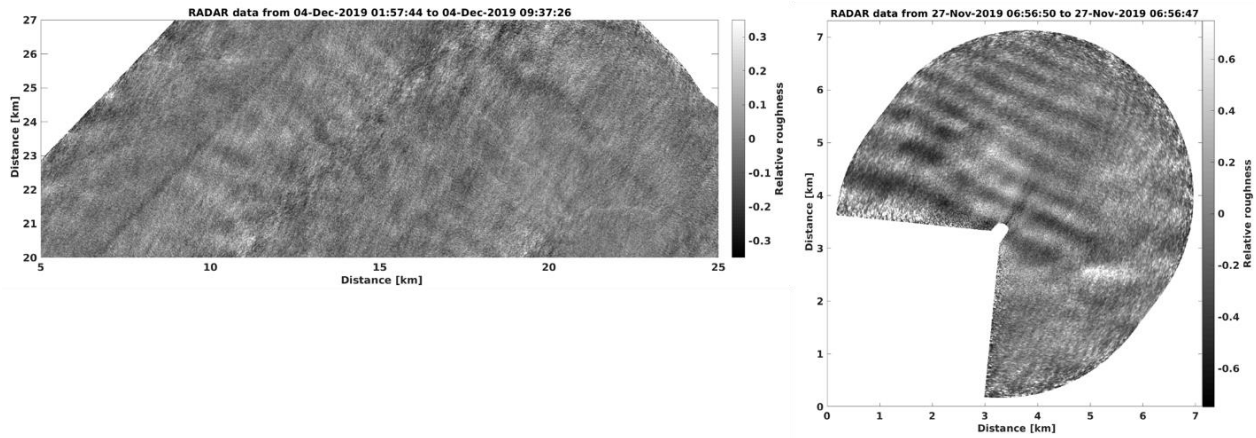


**Figure 5.1.6.1**: Surface front of about 20 km length (left) and internal wave surface features (right) as detected by SuFMoS on 04/12/2019 and from 27/11/2019, respectively.

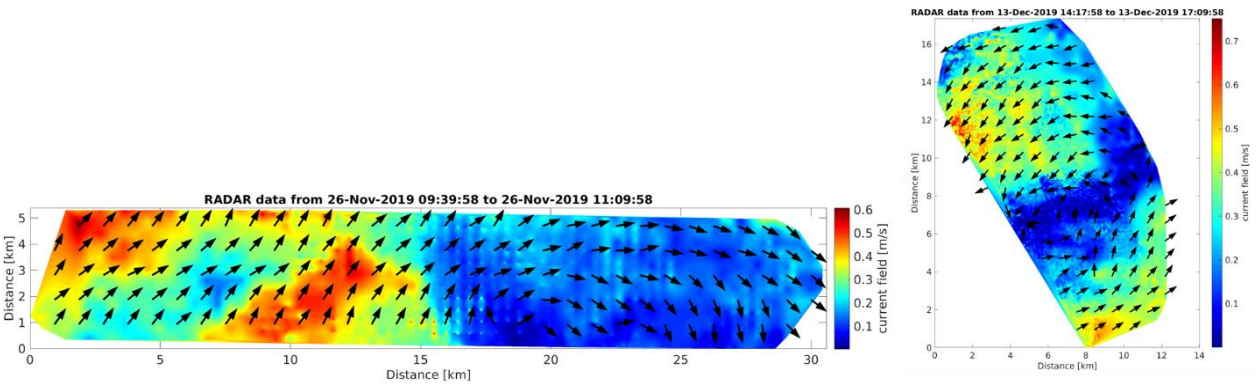


**Figure 5.1.6.2:** 2D current fields extracted during TIA deployments on 26/11/2019 (left) and 13/12/2019 (right), respectively.

## 5.1.7 Glider Operations

(M. Dengler[1], L. Merckelbach[2], L. Schultze[2])

[1]GEOMAR, [2]HZG

A fleet of 12 ocean gliders was an integral component of the measurement program (Table 5.1.7). All gliders were in action during the cruise, except for IFM11, which donated its battery packs to IFM15. Two other gliders (IFM08 and IFM14) were deployed for a pre-cruise survey of the region ahead of the cruise and recovered during the cruise. An overview of the gliders and their sensor configuration is shown in the Table 5.1.7 below.

**Table 5.1.7**: Gliders deployed during M160. Legend: CTD = Seabird 41 CTD, FLNTU = Wetlabs fluorescence and turbidity sensor, Optode = Aanderaa oxygen sensor, MR = Rockland Scientific Microrider system, SUNA = Satlantic nitrate sensor, FL2UrRh = Wetlabs Uranine and Rhodamine sensor, FLBBCD = Wetlabs fluorescence, backscatter and colored dissolved organic matter sensor, OCR504i = Satlantic irradiance sensor.

| Glider name | CTD | FLNTU | Optode | MR | SUNA | FL2UrRh | FLBBCD | OCR504i |
|---|---|---|---|---|---|---|---|---|
| IFM03 | x | x | x | x | | | | |
| IFM08 | x | x | x | | | | | |
| IFM09 | x | x | x | x | | | | |
| IFM12 | x | | x | | x | | x | |
| IFM13 | x | x | x | | x | | x | |
| IFM14 | x | | x | | | x | x | |
| IFM15 | x | | x | | | x | x | x |
| Amadeus | x | x | | | | | | |
| Sebastian | x | | | x | | | x | |
| Comet | x | x | | x | | | | |
| Dipsy | x | x | x | x | | x | | |

All sensors worked as intended, except that the Microriders caused some issues. Two Microriders mounted on Sebastian and Comet did not record useful information due to a programming error that went unnoticed. For a firmware issue with the Microrider mounted on Dipsy a workaround was found, but was not totally successful during operation, causing small gaps during the recording, leaving the data difficult to interpret. The Microrider mounted on IFM09 developed a leak after about three days leading to its early recovery.

The multitude of gliders allowed for gliders to be used in different roles. An overview map with glider trajectories is shown in Fig. 5.1.7 (left). The gliders IFM08 (29/10/2019 - 10/12/2019) and IFM14 (30/10/2019 - 10/12/2019) were used to pre-survey the region north of the Cape Verde, looking for candidate eddies to study in detail during the cruise. Gliders IFM12 and Sebastian (24/11/2019 - 18/12/2019) were deployed in the wind-driven cyclonic eddy southwest of Fogo island. Gliders IFM09 and Comet (26/11/2019 – 18/12/2019) were deployed in the supposedly anticyclonic eddy south of Fogo, and heading west. The research area was moved to the north east, where gliders IFM03, IFM15 (30/11/2019 - 10/12/2019), and Amadeus (30/11/2019 – 5/12/2019) were deployed to assist in pin pointing any frontal structures. Prior to the first dye release experiment also Dipsy was deployed (2/12/2019 - 10/12/2019). During the dye experiment gliders IFM14, IFM15 and Dipsy, which were equipped with the rhodamine sensors, were used to track the dye, where only Dipsy managed to get a few sightings. Upon returning to the southwest region, IFM13, Dipsy (13/12/2019 – 18/12/2019), and IFM15 (14/12/2019 – 18/12/2019) were deployed, where Dipsy and IFM15 tried to track the dye released during the second experiment. During this time, all other remaining gliders were used to survey in detail a frontal region. Due to the high seas and strong winds during the times the gliders were scheduled for recovery, the gliders could not safely be recovered using the Zodiac, and the rescue-star was used instead as last resort. The skilled crew could not prevent that most gliders did not come out unscathed.

Several observational data point to the presence of internal waves in the region. Fig. 5.1.7 (right) shows vertical water velocities observed by glider Comet, computed using a dynamic flight model (Merckelbach et al. 2019) for an east-west transect. Up and downward motion is observed to span over multiple dives, with increased amplitudes in the upper 200 m of the water column. A similar

approach applied to a number of gliders that were within each other's vicinity could yield the directivity of the waves. Furthermore, the data from multiple gliders could contribute to establish a coherent picture of a front surveyed near the island of Fogo. Also, it is expected that the rhodamine concentration observations made by gliders IFM15 and Dipsy provide additional information on the (vertical) dispersion of the dye.

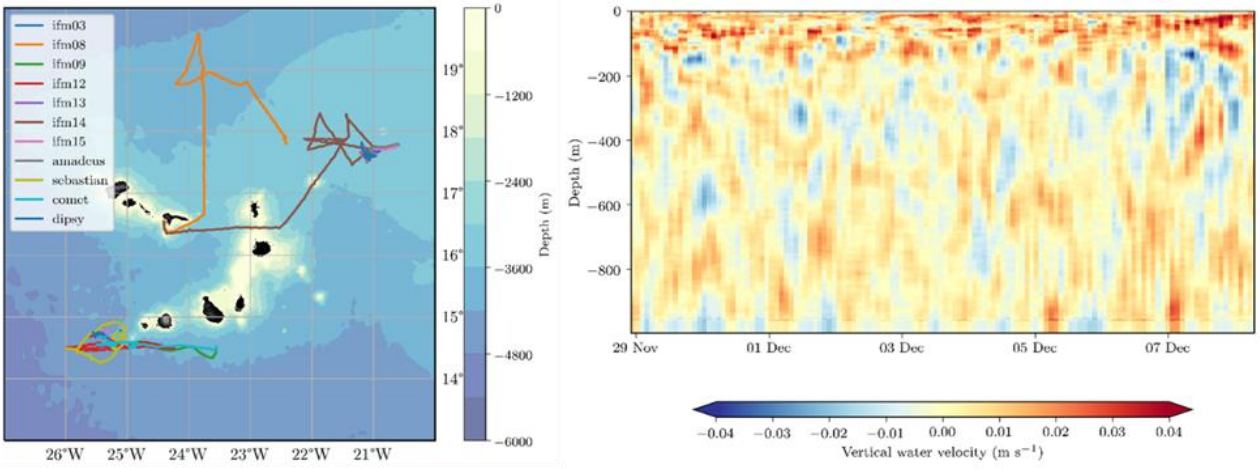


**Figure 5.1.7**: Tracks of all glider deployments during METEOR cruise M160 (left). Vertical water velocities observed by glider Comet, computed for an east-west transect using the dynamic flight model of Merckelbach et al. (2019).

### 5.1.8 Argo Float Deployments

(A. Körtzinger[1], B. Fiedler[1])

[1]GEOMAR

A total of 5 standard Argo floats (Table 5.1.8) were deployed during M160 on behalf of the Bundesamt für Seeschifffahrt und Hydrographie in Hamburg (BSH). Float deployments are a national contribution to the international Argo program.

**Table 5.1.8**: Time and location of standard Argo float deployments during METEOR cruise M160.

| WMO Number | Date and Time UTC | Latitude | Longitude |
|---|---|---|---|
| 7900541 | 2019-11-24 23:32 | 14° 32,119' N | 025° 10,384' W |
| 7900542 | 2019-11-26 19:57 | 14° 29,641' N | 023° 32,018' W |
| 7900743 | 2019-12-01 01:26 | 17° 49,462' N | 020° 36,327' W |
| 7900544 | 2019-12-09 12:50 | 17° 35,500' N | 024° 16,983' W |
| 7900545 | 2019-12-18 21:06 | 17° 35,500' N | 024° 16,983' W |

### 5.1.9 Drifter Deployments

(A. Körtzinger[1], B. Fiedler[1], R. Carrasco[2], J. Horstmann[2])

[1]GEOMAR, [2]HZG

**Surface Velocity Program (SVP) drifters**: A total of 8 MetOcean SVP drifters (Table 5.1.9.1) drifter were deployed during M160 on behalf of the National Oceanic and Atmospheric Administration of USA (NOAA). Drifter deployments were a contribution to the international Global Drifter Program.

**Table 5.1.9.1**: Time and location of SVP drifter deployments during METEOR cruise M160.

| WMO Number | Date and Time UTC | Latitude | Longitude |
|---|---|---|---|
| 3101556 | 24/11/2019 23:40 | 14° 32,390' N | 025° 10,355' W |
| 3101557 | 26/11/2019 19:58 | 14° 29,640' N | 023° 31,991' W |
| 3101558 | 01/12/2019 01:27 | 17° 49,505' N | 020° 36,353' W |
| 3101559 | 09/12/2019 12:52 | 17° 35,580' N | 024° 16,885' W |
| 3101560 | 18/12/2019 21:06 | 14° 22,800' N | 025° 50,657' W |
| 3101561 | 19/12/2019 02:16 | 15° 07,874' N | 025° 42,128' W |
| 3101552 | 19/12/2019 08:18 | 16° 05,284' N | 025° 30,532' W |
| 3101553 | 19/12/2019 12:12 | 16° 44,300' N | 025° 22,843' W |

In addition, two modified SVP Drifter (no WMO classification) were deployed during the first dye release experiment in order to mark and follow the dye streak. Depth of the holey drogues were adjusted to the depth of the dye release. Positions were received directly through the Iridium satellite system via email.

**Mini surface drifter (MDRIFT)** data were collected from MD03i drifters during the cruise starting with the first deployment on 13/12/2019 at 14:10 UTC. Table 5.1.9.2 summarizes positions and times of all mini drifter deployments. Drifter trajectories are shown in Fig. 5.1.9. The drifters were deployed in 3 clusters, containing 3 drifters in each cluster. The MD03i drifters from Albatros Marine Technologies are cylinder shaped with 10 cm in diameter and 32 cm in length. About 8 cm protrude from the water surface and a drogue of both 50 cm length and diameter is attached to each drifter 50 cm below the sea surface so that drifters are supposed to reliably represent currents in a surface layer of about 1 m depth. GPS drifter positions were obtained and transmitted to the vessel via the satellite communication system Iridium. The overall ratio of drag area inside to drag area outside the water is 33.2. Although Albatros MD03i drifters have been widely used during the last years the slippage of this drifter type has never been quantified. However, considering the drag ratio of 33.2, the parameterization given in Niiler et al. (1995) would predict a slippage of 1.1 to 1.6 cm $s^{-1}$ at a wind speed of 10 m $s^{-1}$ and a velocity difference across the vertical extent of the drogue of roughly 0.1 cm $s^{-1}$ (Callies et al. 2019).

**Table 5.1.9.2**: Start and end times and positions of all mini surface drifters deployed during METEOR cruise M160.

| **MDRIFT** | **Start** | | | **End** | | |
|---|---|---|---|---|---|---|
| ID | Time UTC | Latitude | Longitude | Time UTC | Latitude | Longitude |
| ID-02 | 13/12/2019 14:31 | 14.7004 N | 25.3372 W | 07/01/2020 00:54 | 13.8156 N | 27.2750 W |
| ID-03 | 13/12/2019 14:12 | 14.6980 N | 25.3376 W | 01/01/2020 22:37 | 14.6882 N | 25.7498 W |
| ID-04 | 13/12/2019 14:14 | 14.7028 N | 25.3348 W | 29/12/2019 06:55 | 14.4600 N | 25.4802 W |
| ID-05 | 13/12/2019 15:46 | 14.7436 N | 25.3666 W | 13/01/2020 13:00 | 14.6082 N | 29.0430 W |
| ID-06 | 13/12/2019 16:06 | 14.8010 N | 25.3976 W | 21/01/2020 13:42 | 15.6740 N | 29.3674 W |
| ID-07 | 13/12/2019 15:16 | 14.7496 N | 25.3632 W | 03/01/2020 23:41 | 14.2298 N | 26.0536 W |
| ID-09 | 13/12/2019 15:25 | 14.7478 N | 25.3644 W | 03/01/2020 17:04 | 14.2538 N | 26.0236 W |
| ID-13 | 13/12/2019 16:12 | 14.7992 N | 25.3992 W | 07/01/2020 02:41 | 13.8320 N | 26.8290 W |
| ID-15 | 13/12/2019 16:09 | 14.7998 N | 25.3988 W | 09/01/2020 07:26 | 14.1894 N | 25.7512 W |

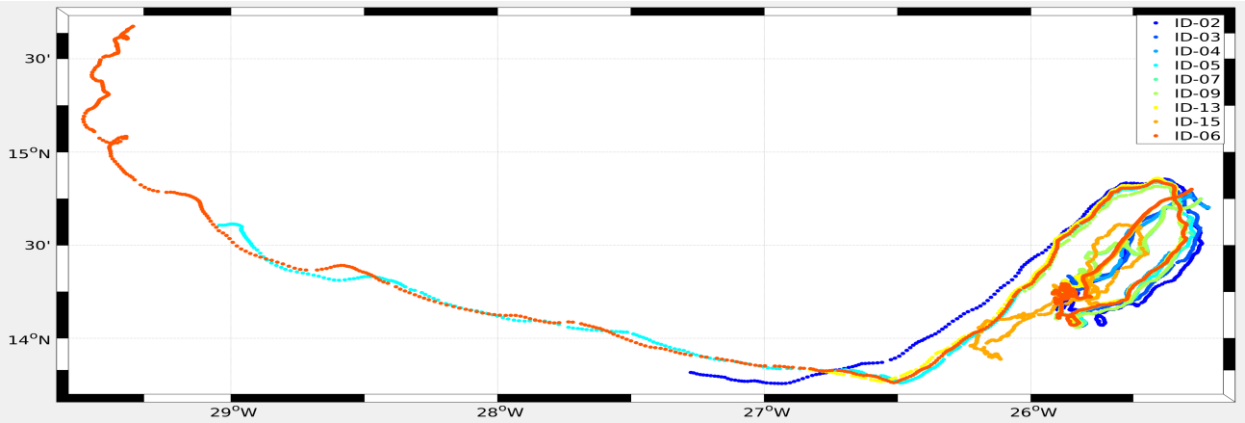


**Figure 5.1.9**: Trajectories of all mini surface drifters deployed during METEOR cruise M160.

### 5.1.10 Short-term Mooring Deployment

(T. Fischer[1], M. Dengler[1], J. Karstensen[1])

[1]GEOMAR

A full-depth mooring was deployed near the core of the strong cyclonic eddy southwest of the islands of Fogo and Brava. The focus of this component of the measurement program was to observe in detail the velocity and hydrographic variability within the cyclonic eddy as well as to obtain reference data from outside of the eddy when it had propagated away from the mooring location.

The mooring was placed in a water depth of 4060 m. Attached sensors included a downward looking Nortek Signature55 acoustic Doppler current profiler at 40 m depth as well as a McLane Moored Profiler (MMP) (Tab. 5.1.10). The MMP recorded 3-D velocity and conductivity, temperature, oxygen and nitrate concentration data while climbing up and down the mooring cable. The climbing depth range was set between 40 m and 1500 m.

The mooring was deployed in the afternoon of 25/11/2019 and retrieved in the afternoon of 16/12/2019. Despite some entanglement of the mooring cable during recovery, both operations went well, largely due to the professionalism of R/V METEOR's boatswain and deck personal.

**Tab. 5.1.10: Deployment, recovery and setup information of mooring KPO 1217.**

| **Mooring Deployment and Recovery** | | | | | **KPO_1217** |
|---|---|---|---|---|---|
| Deployed: | 16/11/2019 | 18:43 UTC | | | |
| Recovered: | 16/12/2019 | 21:13 UTC | | | |
| Latitude: | 14° 32.624' N | Longitude: | 25° 00.304' W | Water depth: | 4060 m |

| **ID** | **Designed depth** | **Instr. type** | **SN** | **Start-up** | **Remarks** |
|---|---|---|---|---|---|
| KPO_1217_01 | 30 m | EOS Argos | 5506 | ready | - |
| KPO_1217_02 | 30 m | SG_ADCP down | S-0065 | x | Complete and clean record |
| KPO_1217_03 | 30 m | MicroCat/p | 10705 | x | Complete and clean record |
| KPO_1217_04 | 34-1500 m | MMP, $O_2$, Suna | ML14754 -01D | x | Profiler operated throughout, surface data missing Conductivity data corrupt Serialnumber Optode (4340) # 2810 Serialnumber SUNA (AG Sommer) #1269 |
| KPO_1217_05 | 4035 m | Release RT661 | 174 | Code: | Enable: 9337 / Release: 9339 |
| KPO_1217_06 | 4035 m | Release AR861 | 110 | Code: | Enable: 0498 / Release: 0455 |

Except of the conductivity sensor, all sensors worked well and provided data. The Nortek Signature 55 sampled velocity in a depth range of more than 1000 m (Fig. 5.1.10). This is a new record for sampled depth range by a moored ADCP from GEOMAR's Physical Oceanography department. The MMP had been ballasted slightly too heavy and therefore experiences problems to reach the upper stopper during the last 10 days. During this period, profiles were usually terminated between 200 m and 300 m depth instead of the 40 m design depth. The MMP collected 238 profiles during the 22 days of deployment.

The velocity data from the ADCP reveal elevated tides and internal wave activity in the southern eddy off Fogo. Semi-diurnal velocity fluctuations (Fig. 5.1.10) indicate the presence of barotropic as well as baroclinic tides with amplitude of more than 0.1 m $s^{-1}$. Additionally, upward sloping phase lines show the presence of down-propagating internal waves having lower frequency compared to the tides. Data analysis in the future will focus on investigating the generation of the internal waves, their interaction with the cyclonic eddy and their impact on upper-ocean mixing processes.

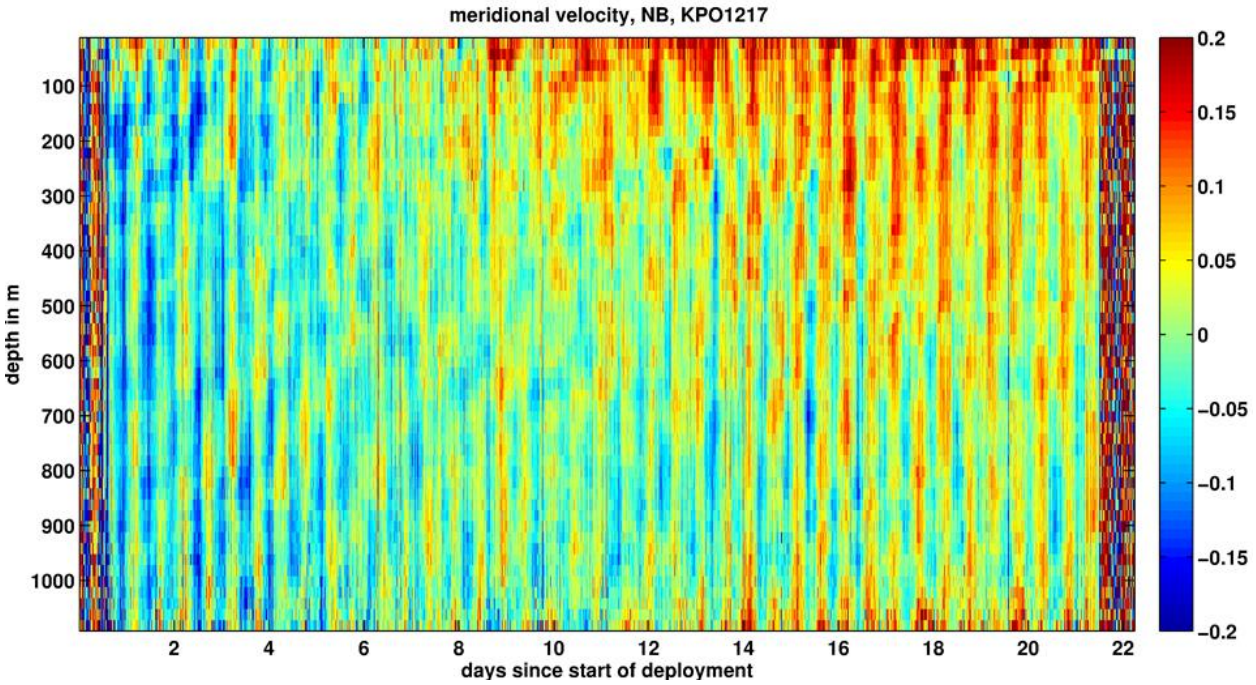


**Figure 5.1.10:** Time series of meridional velocity from the downward looking Nortek Signature55 ADCP. Semi-diurnal tidal currents as well as downward-propagating internal waves are strongly pronounced.

### 5.1.11 Dye Release Experiment

(T. Fischer[1], M. Dengler[1], J. Karstensen[1])

[1]GEOMAR

Two dye release experiments were performed, one per surveyed eddy, to investigate horizontal and vertical spread of dissolved substances at the outer and upper limits of the eddy. The dye streak was placed well below the base of the mixed layer, in order to stay observable for several days and still be able to explore the spread of nutrient-rich water on its way to the mixed layer. The used dye was Rhodamine WT (20% per weight solution), which was mixed with isopropanol and freshwater on board, to adjust the density to the expected target density of seawater. For each experiment, 350 kg of Rhodamine WT (14 barrels, 305 L), 200 L of isopropanol (8 barrels, 157

kg), and 400 L freshwater were mixed with a circulating pump in a 1000 L tank. Taking into account a volume contraction of about 3%, the mixture density fell between 1025 and 1030 kg $m^{-3}$. The mixture density was frequently checked during the mixing process by use of a hydrometer. Without the freshwater, the mixture of Rhodamine and isopropanol is viscous, foamy, can hardly be homogenized, and re-stratifies easily after stopping the circulation pump.

The release of the rhodamine mixture to the target depth was performed using 200 m of wire-reinforced hose connected to a towed sledge which was ballasted with a 500 kg weight. At a ship speed of about 1 kn, the 900 L of prepared dye mixture was pumped past the sledge in about 40 to 50 min. The sledge was equipped with a CTD and a rhodamine fluorometer, so that depth, density and presence of dye could be monitored online. Immediately before and after the dye release, clean seawater from a second 1000 L tank was pumped through the release system. After the second release, the hose was pressure checked at 4 bar, with no leaks detected.

The first dye release was performed at 17°40'N / 21°04' W, on 05/12/2019, 13:34 to 14:16 UTC, in a range of 60 to 68 m in depth, 1026.3 to 1026.4 kg $m^{-3}$ in density, and 16.5 to 17°C in temperature. The second dye release was performed at 14°42' N / 25°23' W, on 14/12/2019, 15:06 to 16:02 UTC, in a range of 48 to 55 m in depth, 1026.3 to 1026.45 kg $m^{-3}$ in density, and 16 to 17.5°C in temperature.

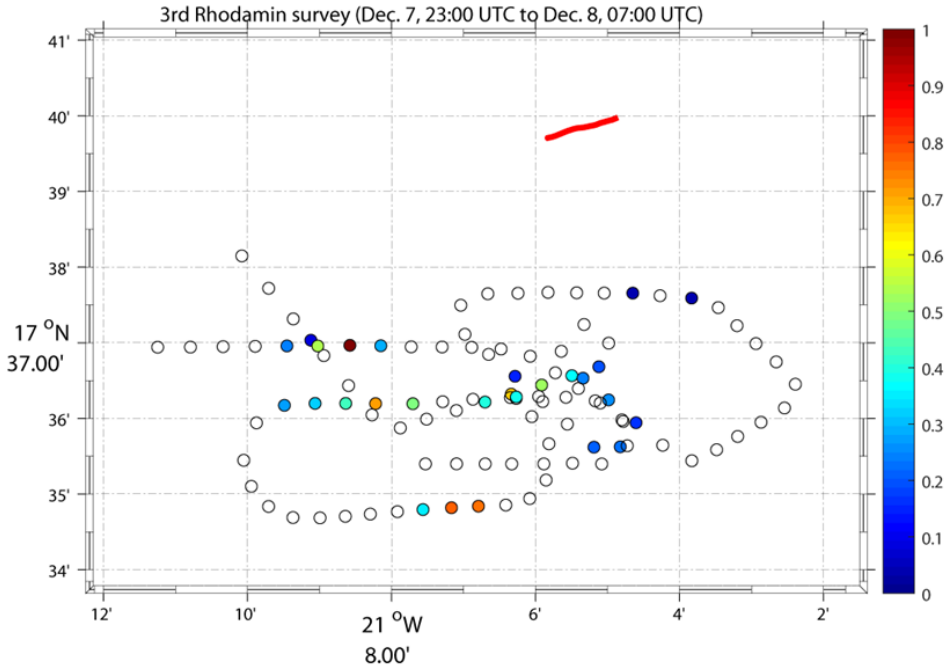


**Figure 5.1.11:** Map of 3rd survey of 1st dye release experiment, about 60 h after release. Maximum column concentrations (µg $L^{-1}$ or ppb) of rhodamine were measured using the Moving Vessel Profiler (MVP) at a ship speed of 7 kn. The red line in the north denotes the initial position of the deployed dye streak.

In order to survey the spreading of the dye patch after release, three different platforms were used: (a) immediately after the release, the TIA (subsection 5.1.2) was equipped with 3 Turner Cyclops rhodamine sensors (practical detection limit 0.2 ppb), one placed at target depth and another one placed each 6 m above and below target depth. This allowed a horizontally dense survey of a small region near the release site, at about 5 kn ship speed. (b) Later, after the dye streaks could be expected to be wider than a few hundred meters, the Moving Vessel Profiler (subsection 5.1.1.4, Fig. 5.1.11) was used, performing frequent profiles down to 90 m with a Turner C-Fluor

rhodamine sensor (practical detection limit 0.04 ppb). At a ship speed of maximum 8 kn, a speed dependent profile spacing of 300 m to 1000 m could be achieved. The main advantage of the MVP is the acquisition of high-resolution profiles of rhodamine, so that dye detection could be performed independent of internal wave activity and correct estimate of target depth. (c) As an accompanying measurement, and for times when the vessel could not be on site, two gliders equipped with Wetlabs rhodamine sensors (practical detection limit 0.15 ppb) were surveying the region of the dye patch expected location.

## 5.2 Marine Biogeochemistry, Chemical & Biological Oceanography

### 5.2.1 Discrete Seawater Sampling

(B. Fiedler[1], M. Paulsen[1], T. Hahn[1], A. Körtzinger[1], A. Engel[1], H. Hepach[1], K. Becker[1], Q. Devresse[1], S. Golde[1], L. Hufnagel[2], M. Iversen[2,3])

[1]GEOMAR, [2]MARUM, [3]AWI

A diverse suite of discrete water samples was collected during the cruise from both vertical CTD/RO hydrocasts (chapter 5.1.1.1) and the seawater underway system (chapter 5.2.2). Biogeochemical and biological parameters were used to investigate spatial distributions in- and outside mesoscale eddies to better understand biogeochemical cycling of carbon, nitrogen and oxygen across eddy boundaries (see example in Fig. 5.2.1). Biogeochemical samples were also used to calibrate CTD and underway biogeochemical sensors.

Biological parameters associated with organic matter were sampled in order to investigate the influence of (sub)mesoscale eddies formed in EBUS regions on (i) upper ocean organic carbon distribution, (ii) microbial productivity and organic matter turn-over and (iii) supply of organic matter to the central Atlantic Ocean. To relate the composition and bacterial diversity of sinking aggregates to the occurrence and abundance of phytoplankton and heterotrophic organisms in the water column, water samples corresponding to all drifting sediment trap stations (chapter 5.2.7) were taken with a CTD/RO Niskin water sampler.

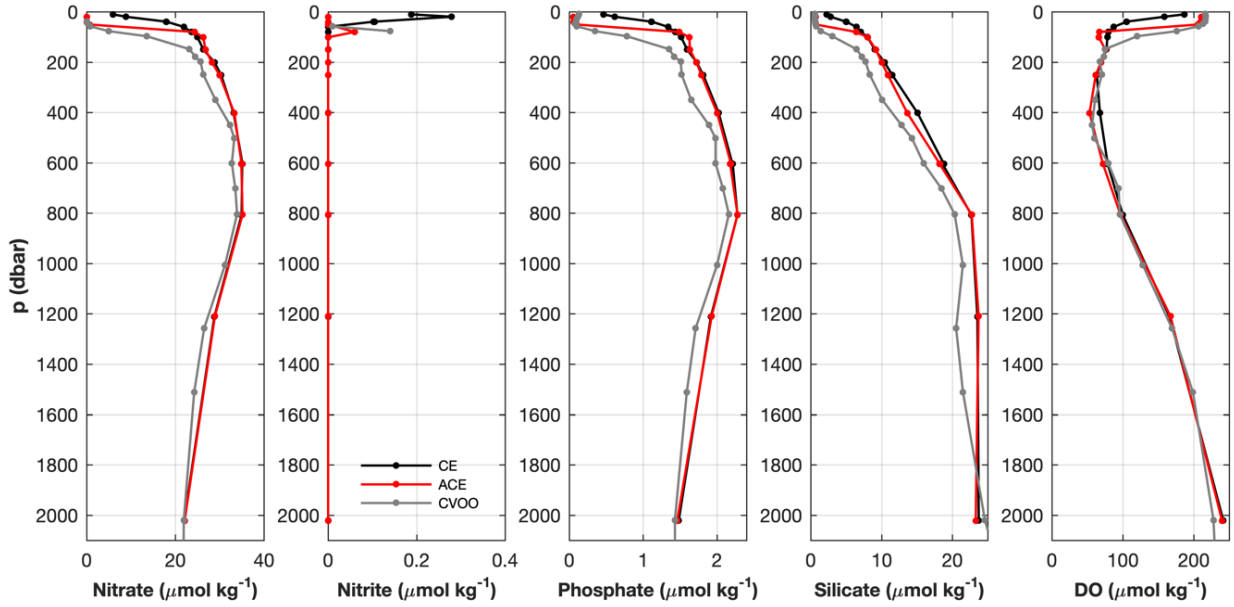


**Figure 5.2.1.1:** Vertical profiles for dissolved inorganic nutrients and DO in the cyclonic eddy (CE) southwest of the island of Fogo, an anticyclonic eddy (ACE) south of the island of Santiago, and at the CVOO time series site 60 nm northeast of the island of São Vicente (no eddy).

**Dissolved Oxygen (DO)** was semi-automatically determined by using the Winkler method with visual (starch) endpoint detection within a minimum (maximum) of 48 min (16 h) after sampling, following standard protocols in Grasshoff et al. (1999, chap. 4: Determination of oxygen). Samples were taken with 100 mL wide-necked WOCE glass bottles with well-defined volumes (calibrated flasks with matched pair of flask and stopper) and always at first from the CTD/RO, while sample bottles were flushed with 3 times its volume. At each CTD/RO cast, at least one replicate from one of the Niskin bottles was taken in order to quantify sampling and titration uncertainties. Titrations were performed within the WOCE bottles using a 20 mL TITRONIC universal Piston Burette (SN 693123), whereas the iodate standard was added with a 50 mL TITRONIC universal Piston Burette (SN 693160), both from SI Analytics GmbH. Of each fixation solution, 1 mL was added with a high precision bottle-top dispenser (0.4 - 2.0 mL, Ceramus classic, Hirschmann). All reagents corresponded to those in Grasshoff et al. (1999), except that a commercial zinc iodide starch solution was utilized (500 mL, Merck KGaA). A minimum of 3 standard measurements for the determination of the thiosulfate factor were carried out on each sampling day. Every newly prepared standard solution (homemade, pre-weighted $KH(IO_3)_2$) was carefully validated against a CSK standard solution (potassium iodate) from FUJIFILM Wako Chemicals Europe GmbH. The relative difference of both sodium thiosulphate factors was 0.237% on average, and were continuously between 0.9980040 and 1.0020040 (ideally 1). The reagent blank (resulted in a difference of $a_r$ = -0.005 mL (arithmetic mean).

A total of 865 discrete water samples were taken from selected depths of 67 CTD casts (average 10.81 samples/cast). Note that the bottle factor of flask 30 was asserted erroneous, thus all associated values for DO are incorrect. After such quality control checks, a total of 842 samples were declared valid. DO concentrations were calculated according to the GO-Ship SOP (Langdon, 2010) and varied between 39.45 (minimum) and 247.73 (maximum) µmol $L^{-1}$. Additional 37 water samples were analyzed from the underway system (see chapter 5.2.2 for further detail). The precision (arithmetical averages of all standard deviations per replicate) of the Winkler-titrated oxygen measurements (1 σ) was 0.33 µmol $L^{-1}$ based on 84 replicates (81 triplicates, 2 duplicates and 1 sextuplet).

**Dissolved inorganic carbon and total alkalinity:** A total of 443 samples from the CTD/RO and 33 from the underway seawater system (chapter 5.2.2) were collected in 250 mL glass bottles with glass stoppers for analysis of dissolved inorganic carbon (DIC) and total alkalinity (TA). The sampling procedure and preservation (mercury chloride) of samples followed the recommendations from (Dickson et al. 2007). All samples were stored in the dark after sampling. Onshore DIC samples will be analyzed with a coulometric titration method using the SOMMA (Single-Operator Multiparameter Metabolic Analyzer). The SOMMA collects and dispenses an accurately known volume of seawater to a stripping chamber, acidifies it, sparges the $CO_2$ from the solution, dries the gas, and delivers it to a coulometer cell, where the $CO_2$ reacts with an ethanolamine solution forming an acid that is titrated with in-situ produced $OH^-$ ions. The amount of electricity required to titrate all acid formed is precisely monitored (coulometry) and corresponds to the amount of $CO_2$ released from the sample. TA will be determined by a semi-automatic analyzer, the VINDTA (Versatile Instrument for the Determination of Titration Alkalinity). This instrument determines TA by titration of seawater with a strong acid, following the EMF of a proton sensitive electrode.

**Nutrient measurements:** Nutrients were measured on board with a QuAAtro autoanalyzer from SEAL Analytical (SN 8003836) and a SEAL XY-2 autosampler (SN 5002A15014). The following methods from SEAL Analytical were used:

- Nitrate via nitrite (Q-068-05 Rev. 7): The nitrate is determined as nitrite after reduction on a cadmium coil. The nitrite is determined with a colorimetric method where sulphanilamide is forming a diazo compound.
- Nitrite (Q-070-05 Rev. 6): The nitrite is determined with a colorimetric method where sulphanilamide is forming a diazo compound.
- Phosphate (Q-064-05 Rev. 4): Phosphate is determined with a colorimetric method based on reaction with molybdate and antimony ions.
- Silicate (Q-066-05 Rev. 3): Silicate is determined with a colorimetric method where a silico-molybdate complex is reduced to molybdenum blue.

Altogether 858 nutrient samples from 66 CTD/RO casts were sampled during the cruise, of which 104 samples were taken as triplicates. The 14 mL polyethylene sampling tubes and the respective caps were rinsed at least three times with the sampling water before the actual sample was taken. In most cases, the samples were measured within 6 h after sampling. If the start of measurement was delayed for more than 1 h, the samples were stored in the fridge in the meantime. The precision of the nutrient measurements as calculated from the triplicate analyses is given in Table 5.2.1.1:

**Table 5.2.1.1**: Precision of nutrient measurement as calculated from triplicate analyses.

| Analyte | Precision (µmol $L^{-1}$) |
|---|---|
| Nitrate (via nitrite) | 0.155 |
| Nitrite | 0.003 |
| Phosphate | 0.008 |
| Silicate | 0.065 |

In addition to the CTD/RO samples, a total of 6 bottles of certified reference material (CRM) for nutrients in Seawater (RMNS) from the General Environmental Technos (KANSO) Co., Ltd., Osaka/Japan, were measured as triplicates at least once per run. The nutrient concentration of the CRM from lot CH and the standard deviation of the measured CRM replicates is given in Table 5.2.1.2:

**Table 5.2.1.2**: Known nutrient concentration ($C_{ref}$, ± 1 SD) and calculated concentration in volumetric unit ($C_{calc}$, ± 1 SD) of the certified reference material for nutrients in seawater are listed. The standard deviation (SD) of the CRM replicate measurements are also shown.

| Analyte | $C_{ref}$ (µmol $kg^{-1}$) | $C_{calc}$ (µmol $L^{-1}$) | SD (µmol $L^{-1}$) |
|---|---|---|---|
| Nitrate | 16.94 ± 0.15 | 17.36 ± 0.15 | 0.044 |
| Nitrite | 0.159 ± 0.015 | 0.159 ± 0.015 | 0.002 |
| Phosphate | 1.172 ± 0.015 | 1.201 ± 0.015 | 0.005 |
| Silicate | 30.0 ± 0.3 | 30.8 ± 0.3 | 0.104 |

**Particulate and dissolved organic matter:** At 31 CTD/RO stations from two cyclonic eddies water samples were collected for: (i) dissolved organic matter (DOM) analysis including dissolved organic carbon (DOC), total dissolved nitrogen (TDN), dissolved organic phosphorous (DOP),

chromophoric dissolved organic matter (CDOM), fluorescent dissolved organic matter (FDOM), dissolved combined carbohydrates (dCCHO) and dissolved amino acids (dAA); (ii) non-sinking organic matter components, such as transparent exopolymeric particles (TEP) and coomassie stainable particles (CSP) following the procedures described in Alldredge et al. (1993) and Long and Azam (1996); (iii) particulate organic matter (POM) analysis including particulate organic carbon (POC) content as well as pigment and lipid compositions; (iv) analysis of the abundance, distribution and community structure of pico- and nano phytoplankton as well as bacteria and viruses using flow cytometry; (v) microbial process rates including primary production, heterotrophic biomass production and aerobic microbial respiration. We collected a total of 168 samples (in replicates) for all DOM and POM parameters as well as for flow cytometry. For the microbial process rates, fewer samples were collected because of the more time-consuming sample processing, which includes incubations. See Table 5.2.1.3 for a list of the collected discrete water samples.

All DOM, POM, non-sinking organic matter and flow cytometry samples were shipped cooled or frozen to GEOMAR for further analysis in the Engel lab at GEOMAR, while microbial process rates were determined on board. To determine primary production and release rates of organic carbon by phytoplankton, $^{14}C$ uptake measurements were conducted according to Steemann Nielsen (1952) and Gargas (1975). Microbial heterotrophic biomass production was determined using the $^{3}H$-leucine incubation method (Kirchman et al. 1985, Smith and Azam 1992). Bacterial respiration was determined during bioassays applying oxygen optodes following the protocol described in Vikström et al. (2019).

**Phytoplankton and bacterial communities:** Sampling was done at drifting sediment trap depths (chapter 5.2.7) at 400 m, 200 m and 100 m, two mixed layer depths depending on the chlorophyll profile and at 10 m in the surface. Samples for identification of phytoplankton and samples for catalyzed reporter deposition fluorescence in situ hybridization (CARD-FISH) were fixed with 1% formaldehyde and stored at 4°C and -20°C, respectively, to assess the phytoplankton and free-living bacterial community quantitatively. Additionally, between 1.5 and 3.5 L of water were size-fractionated for taxonomic identification of phytoplankton (polycarbonate filters of 10 µm, 3 µm and 0.4 µm pore size) and of the bacterial community (polycarbonate filters of 3 µm and 0.2 µm pore size). The amount of water filtered was depending on the amount of material present in the water column at the respective depths. The filters were then stored at -20°C for processing in the home laboratory.

## 5.2.2 Underway Biogeochemical Measurements

(M. Paulsen[1], B. Fiedler[1], A. Körtzinger[1])

[1]GEOMAR

A variety of autonomous measurements were conducted over the entirety of this cruise by using a flow-through setup (Fig. 5.2.2). For this purpose, a pump (Scuba SC205C, Xylem Water Solutions Deutschland GmbH, Großostheim, Deutschland) was installed at approx. 5 m depth in the ship's moon pool pumping seawater to a manifold supplying the different underway systems and a tap for taking discrete samples. In total, 139 discrete reference samples were taken for quality control of the sensor measurements.

One seawater outlet supplied a system for continuous $pCO_2$ measurements (General Oceanics, Miami, USA) following the design described by Pierrot et al. (2009). Due to the failure of an AD converter, the autonomous calibration of the infrared gas analyzer was impossible, hence an analog routine was established with a calibration approximately every 8 h. The LabVIEW software controlling the instrument was replaced with a MATLAB script collecting the sensor data.

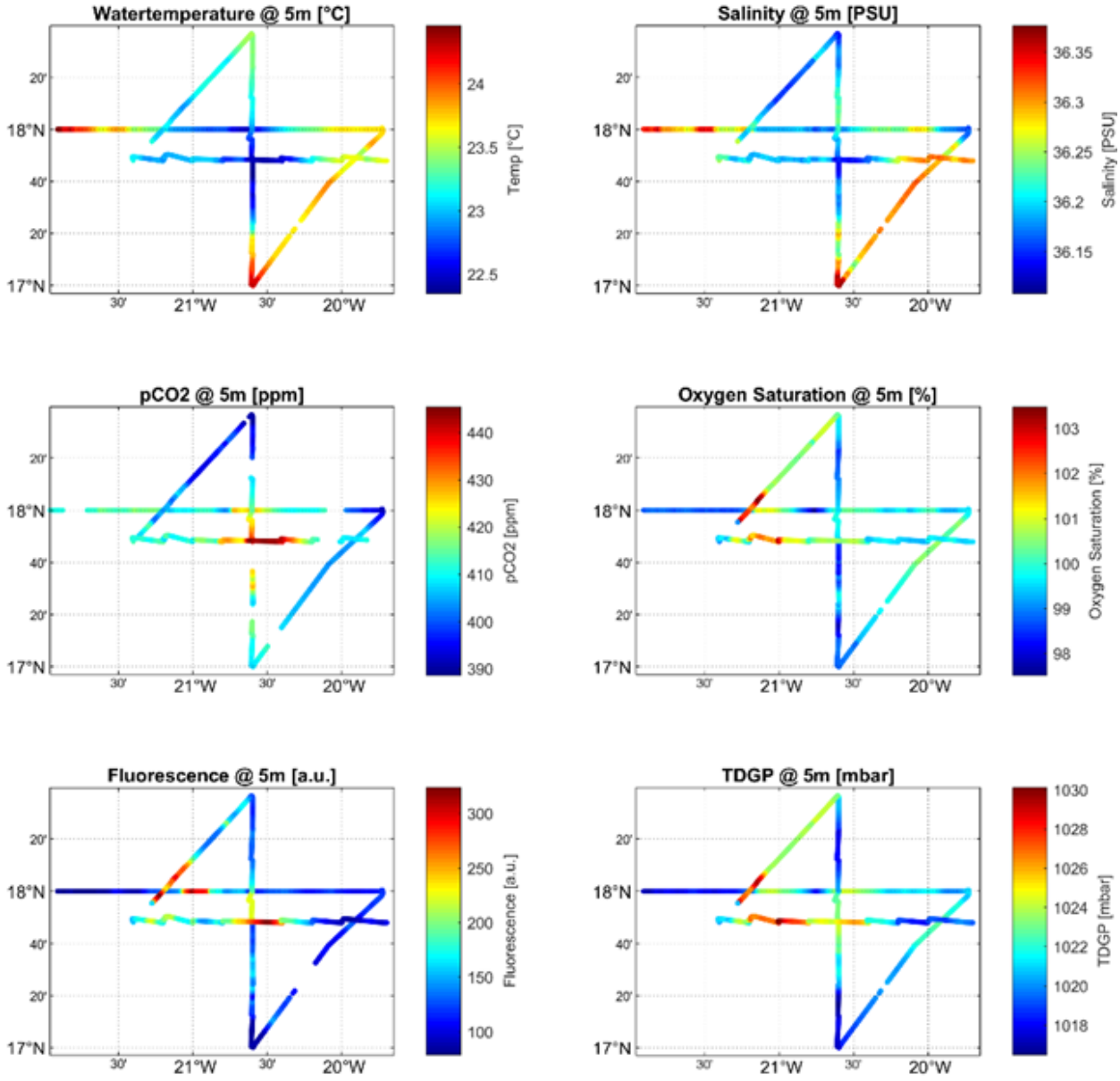


**Figure 5.2.2**: Example of unprocessed biogeochemical underway data from the transect through the cyclonic eddy northeast of the island of Sal ("Eddy 2").

Another seawater outlet supplied a flow-through cooling container housing multiple submerged sensors. All sensors were connected to a single computer where data were logged using a MATLAB script. Water within the container was routed to a total gas tension sensor (HGTD, Pro-Oceanus Systems Inc., Halifax, Canada, SN 3316916) and a dissolved oxygen sensor (SBE 63, Sea-Bird Electronics, Bellevue, USA, SN 631783) using a pump (SBE5T, Sea Bird Electronics, Bellevue, USA). A conductivity sensor (4319A, Aanderaa Instruments AS, Bergen, Norway, SN

4319-772), a two-channel fluorometer (FLNTURT, Sea Bird Electronics, Bellevue, USA, SN 4899) measuring turbidity and fluorescence and an oxygen optode (HydroFlash $O_2$, KM Contros GmbH, Kiel, Germany, SN DO-0216-004) were directly exposed to the water in the flow-through container. Additionally, a temperature sensor (SBE 38, Sea-Bird Electronics, Bellevue, USA, SN 3847374 0366) was installed in the moon pool next to the pump.

### 5.2.3 Marine Snow Sampling (MSC)

(N. Moradi[1], L. Hufnagel[1], G. Fischer[1], M. Iversen[1,2], C. Flintrop[2], K. Becker[3], Q. Devresse[3], H. Hepach[3], S. Golde[3], A. Engel[3])

[1]MARUM, [2]AWI, [3]GEOMAR

The fraction of organic matter that leaves the upper mixed layer of the ocean is, among other factors, determined by the sinking velocity, composition, size and turnover (by microbes and zooplankton) of sinking aggregates. In order to determine the efficiency of the biological carbon pump, it is therefore important to determine the size-specific composition and sinking velocity of marine aggregates since this directly determines the amount of carbon that can be transported vertically through the water column. We used two Marine Snow Catchers (MSC, OSIL) to collect in situ formed marine aggregates (Table 5.2.3). Samples were typically collected from about 10-20 m below the chlorophyll maximum (as seen from the chlorophyll sensor readings of the preceding CTD/RO cast). After deployment (Fig. 5.2.3.1a), aggregates collected in the 100 L sampler volume were left to settle to the base of the MSC on deck for about 3 h. At each station, one MSC was used for individual aggregate sampling (Fig. 5.2.3.1b) and the second MSC was used for bulk aggregate sampling. Individual particles were gently collected using a wide-mouth bore pipette and transferred to a flow chamber system equipped with an $O_2$ microsensor for onboard measurements of aggregate size, sinking velocity and microbial respiration (see Ploug and Jørgensen (1999) for further detail).

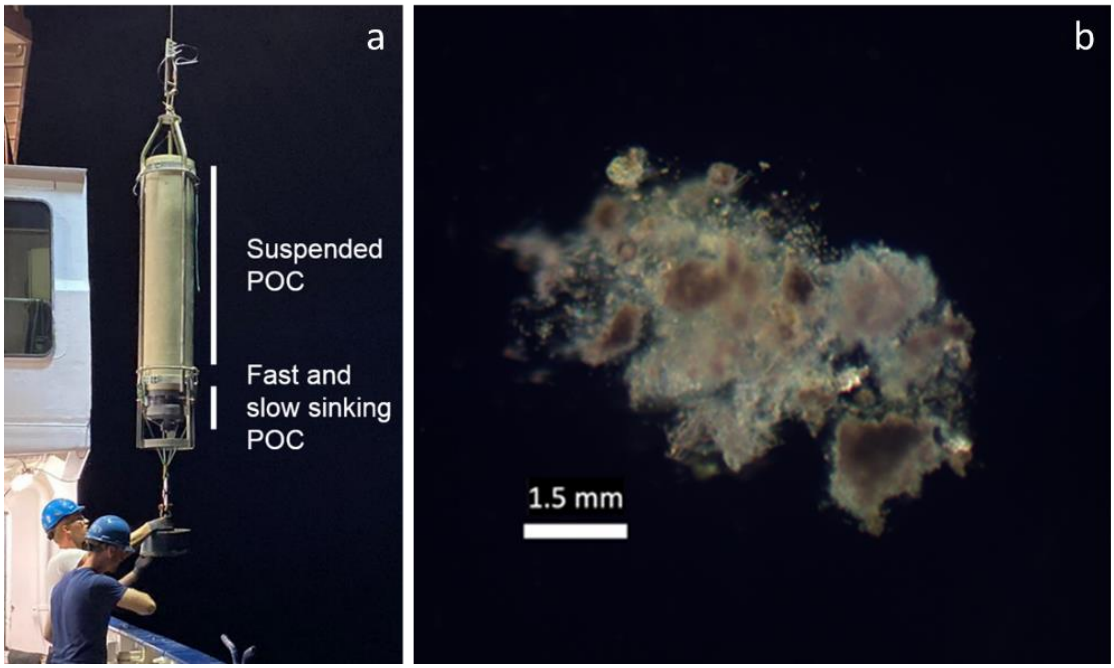


**Figure 5.2.3.1**: (a) Deployment of the MSC during M160. (b) Microscope image of an aggregate sampled from the base of the MSC.

**Table 5.2.3**: Times and positions of Marine Snow Catcher deployments during M160.

| Station No. | Date UTC | Time UTC | Sampling depth (m) | Water depth (m) | Latitude (°) | Longitude (°) | Location |
|---|---|---|---|---|---|---|---|
| M160-13-1 | 25/11/19 | 20:25 | 20 | 4297 | 14° 28.999' N | 025° 02.986' W | Eddy 1 (center) |
| M160-14-1 | 25/11/19 | 20:36 | 20 | 4292 | 14° 29.000' N | 025° 02.984' W | Eddy 1 (center) |
| M160-53-1 | 30/11/19 | 18:43 | 40 | 3139 | 17° 47.962' N | 020° 36.022' W | Eddy 2 (center) |
| M160-54-1 | 30/11/19 | 19:07 | 40 | 3139 | 17° 47.963' N | 020° 36.024' W | Eddy 2 (center) |
| M160-71-1 | 01/12/19 | 15:51 | 40 | 3212 | 18° 36.579' N | 020° 36.399' W | Eddy 2 (north rim) |
| M160-72-1 | 01/12/19 | 16:05 | 40 | 3212 | 18° 36.579' N | 020° 36.400' W | Eddy 2 (north rim) |
| M160-91-1 | 03/12/19 | 03:17 | 60 | 3154 | 17° 48.880' N | 020° 24.541' W | Eddy 2 (center) |
| M160-92-1 | 03/12/19 | 03:29 | 60 | 3155 | 17° 48.880' N | 020° 24.542' W | Eddy 2 (center) |
| M160-112-1 | 06/12/19 | 20:41 | 60 | 3204 | 17° 49.327' N | 021° 14.191' W | Eddy 2 (west rim) |
| M160-113-1 | 06/12/19 | 20:57 | 60 | 3204 | 17° 49.413' N | 021° 14.380' W | Eddy 2 (west rim) |
| M160-144-1 | 12/12/19 | 19:43 | 60 | 2516 | 14° 37.313' N | 024° 54.459' W | Eddy 1 (outside) |
| M160-145-1 | 12/12/19 | 19:55 | 60 | 2501 | 14° 37.576' N | 024° 54.364' W | Eddy 1 (outside) |
| M160-177-1 | 15/12/19 | 03:17 | 40 | 4417 | 14° 43.252' N | 025° 29.341' W | Eddy 1 (center) |
| M160-178-1 | 15/12/19 | 03:29 | 40 | 4418 | 14° 43.251' N | 025° 29.341' W | Eddy 1 (center) |
| M160-186-1 | 16/12/19 | 07:28 | 60 | 4507 | 14° 38.486' N | 025° 46.799' W | Eddy 1 (south rim) |
| M160-187-1 | 16/12/19 | 07:40 | 60 | 4509 | 14° 38.226' N | 025° 47.071' W | Eddy 1 (south rim) |

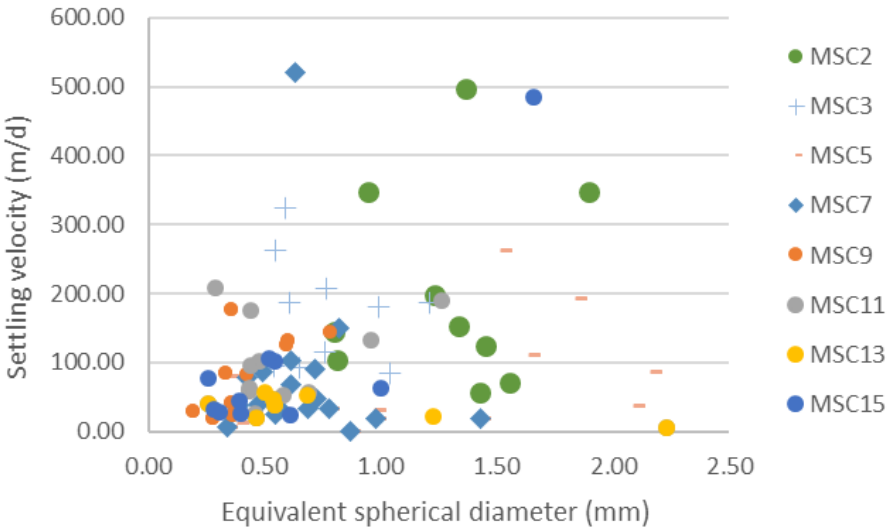


**Figure 5.2.3.2**: Sinking velocity of collected marine aggregates versus aggregate size (ESD = Equivalent Spherical Diameter).

We measured the size and settling velocity of 98 aggregates in total. The majority of aggregates were smaller than 1 mm and sank with a velocity of approximately 100 m $d^{-1}$. There was no apparent correlation between aggregate size and settling velocity (Fig. 5.2.3.2). Preliminary analysis of microsensor measurements revealed that microbial respiration (and therefore microbial degradation) in the examined eddies was low. From the flow chamber, aggregates were transferred to 1 mL microcentrifuge tubes and frozen at -20°C for analysis of particulate organic carbon content or associated microbial assemblages in the home laboratory. For bulk characterization, aggregates were transferred to a beaker with a 5 mL serological pipette. The bulk sample was then equally split into subsamples for analysis of the parameters listed below. Additionally, suspended

POC samples were collected from the upper part of the snow catcher to compare measurements from the aggregates with the surrounding waters. Bulk aggregate and suspended samples were stored cooled or frozen and shipped to GEOMAR for analysis. Together the MSC sampling provided in situ (i) aggregate composition, size, settling velocity, microbial respiration rate, microbial community composition, and particulate organic carbon content of individual aggregates and (ii) particulate organic carbon and nitrogen (POC/N), particulate organic phosphorus (POP), lipids, amino acids (AA), combined carbohydrates (CHO), transparent exopolymeric particles (TEP), Coomassie-stainable particles (CSP), confocal laser scanning microscopy (CLSM), bacterial biomass production (BBP), and flow cytometry of bulk aggregate samples. The aim of sampling marine snow in situ is to comprehensively characterize the chemical composition, sinking behavior, and microbial assemblages of aggregates in low oxygen.

### 5.2.4 Profiling Optical Observations (UVP, CPICS)

(H. Hauss[1], D. Blandfort[2])

[1]GEOMAR, [2]HZG

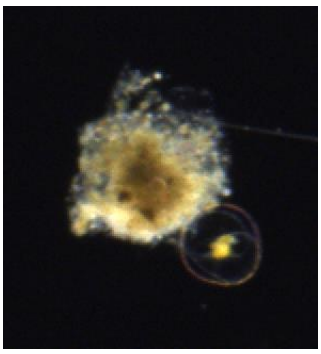

**Underwater Vision Profiler** (UVP) and **Continuous Plankton Imaging and Classification System** (CPICS):

To study the composition, distribution and dynamics of plankton and marine snow, two *in situ* camera systems were mounted on the CTD/RO, the Underwater Vision Profiler UVP5 (Picheral et al. 2010) and the Continuous Plankton Imaging and Classification System CPICS (Gallager 2016). The CPICS is capable of taking color (darkfield) images within a size spectrum from a few µm up to several cm, while the UVP5 acquires greyscale images and directly processes the abundance of particles starting at a pixel size of approximately 30µm. A dedicated stand-alone CTD was directly connected to the CPICS to be able to match each image with the respective hydrographic information via timestamp. The UVP5 data (particle abundance in different size bins as well as image data) will be matched to calibrated CTD/RO profiles and are stored and sorted into taxonomic categories using Ecotaxa (https://ecotaxa.obs-vlfr.fr/). After taxonomic classification and in-depth analysis of the data, small-scale distribution of different types of particles and species will be available.

### 5.2.5 Biogeochemical Argo Float Deployments (BGC-Argo)

(B. Fiedler[1], A. Körtzinger[1])

[1]GEOMAR

In order to extend biogeochemical observations in individual eddies and to investigate underlying variability with an enhanced temporal resolution 3 BGC Argo floats (Table 5.2.5) were deployed during the cruise. Floats were equipped with standard SBE41N CTD caps, Aanderaa oxygen optodes 4330 and Wetlabs ECO_FLBBCD fluorometers. In addition, two floats (7900559 and 7900560) were equipped with Seabird SEAFET pH probes and one float (7900561) with a Satlantic OCR504 radiometer. All floats were programmed to carry out profiles every 36 h with a maximum depth of 1200 m and a parking depth of 200 m. A shallow parking depth was chosen in order to enhance the likelihood of the floats to stay inside an eddy for a longer period. CTD/RO

hydrocast incl. biogeochemical sampling were carried out nearby deployment locations for reference.

**Table 5.2.5**: Time and location of BGC Argo float deployments during METEOR cruise M160.

| WMO Number | Date and Time UTC | Latitude | Longitude |
|---|---|---|---|
| 7900559 | 2019-11-24 23:37 | 14° 32,306' N | 025° 10,358' W |
| 7900560 | 2019-12-01 01:16 | 17° 49,162' N | 020° 36,155' W |
| 7900561 | 2019-12-01 01:22 | 17° 49,365' N | 020° 36,269' W |

### 5.2.6 Wave Glider Operations

(B. Fiedler[1], M. Paulsen[1], A. Körtzinger[1])

[1]GEOMAR

Continuous measurements of biogeochemical parameters in the ocean's surface were carried out using two wave gliders of Liquid Robotics, Inc. (Sunnyvale, USA) one being the SV2 version (SN 003522) the other one the newer SV3 version (SN SV3-193). Both Wave Gliders were equipped with a BGC sensor package consisting of a $pCO_2$ Sensor (HydroC®, Contros, Kiel, Germany, SN CO2-1117-001 (SV3), SN CO2-0412-012 (SV2)), an oxygen sensor (SBE63, Sea Bird Electronics, Bellevue, USA, SN 63-0392 (SV3), 63-0492 (SV2)), a two channel fluorometer (FLNTURT, Sea Bird Electronics, Bellevue, USA, SN 2493 (SV3), 2768 (SV2)) measuring turbidity and fluorescence and a sensor to measure the total gas pressure of all dissolved gases (SV3: Mini TDGP, Pro-Oceanus Systems Inc., Halifax, Canada, SN 38 511 31; SV2: HGTD, Pro-Oceanus Systems Inc., Halifax, Canada, SN 3316916). The SV3 Wave Glider was additionally equipped with an ADCP (300 kHz Workhorse, RD Instruments, Poway, USA, SN 1962) and the SV2 with an echo sounder (Simrad EK 15, Kongsberg Maritime, Kongsberg, Norway).

Deployment of the SV3 Wave Glider was carried out already prior to METEOR cruise M160 on 29/10/2019 with the Cape Verdean Coast Guards patrol vessel Guardião southwest of São Nicolau in the Bay of Tarrafal. The Wave Glider conducted a pre-cruise survey of a possible research region north of the Cape Verdean Islands mainly focusing on ADCP measurements. It was recovered on 02/12/2019 to remove the $pCO_2$ sensor and redeployed the same day. It was again recovered on 10/12/2019 to relocate to the new operational region southwest of Fogo island, where it was deployed on 12/12/2019. The final recovery took place on 16/12/2019. The SV2 Wave Glider was deployed from RV Meteor 24/11/2019 southwest of Fogo island and stayed in the region until its recovery 17/12/2019.

Examples of the data collected with SV2 and SV3 Wave Gliders are shown in Figs. 5.2.6.1, 5.2.6.2, and 5.2.6.3.

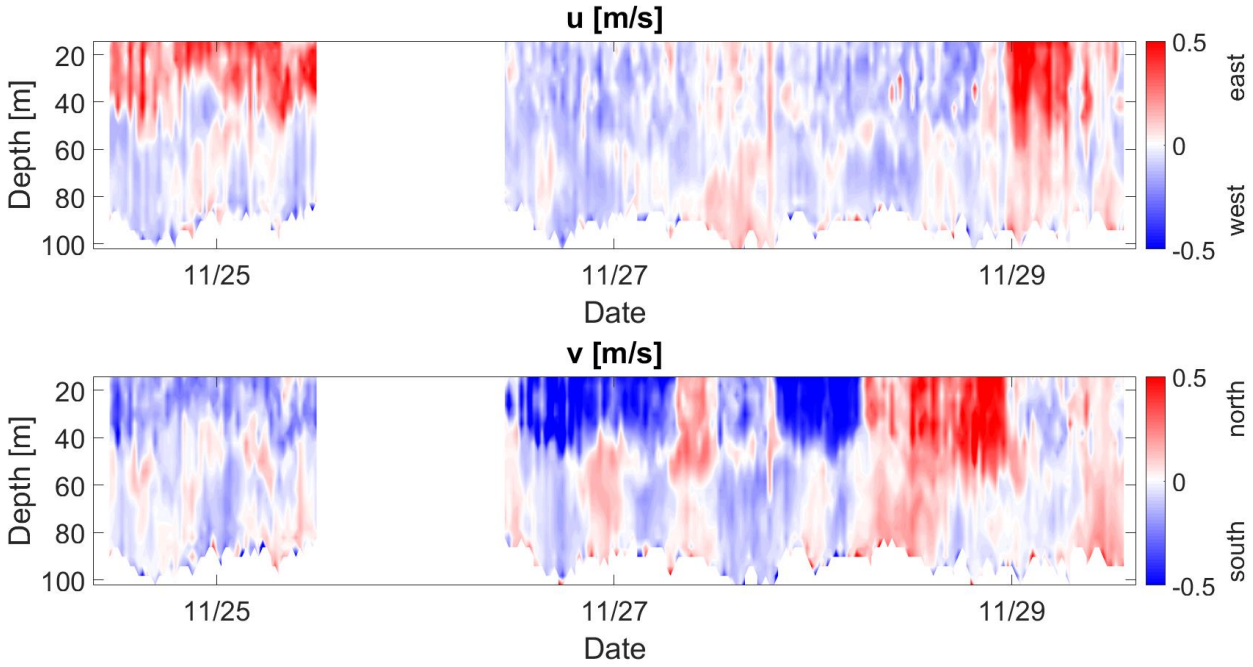


**Figure 5.2.6.1:** ADCP telemetry data received from the SV3 Wave Glider during METEOR cruise M160.

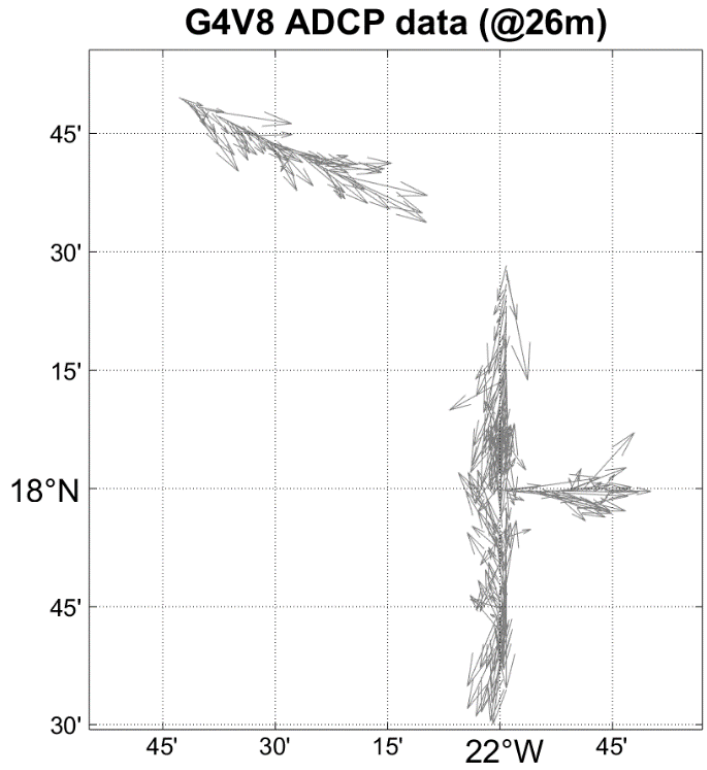


**Figure 5.2.6.2:** Example of current vectors derived from Wave Glider ADCP data for a water depth of 26 m during METEOR cruise M160.

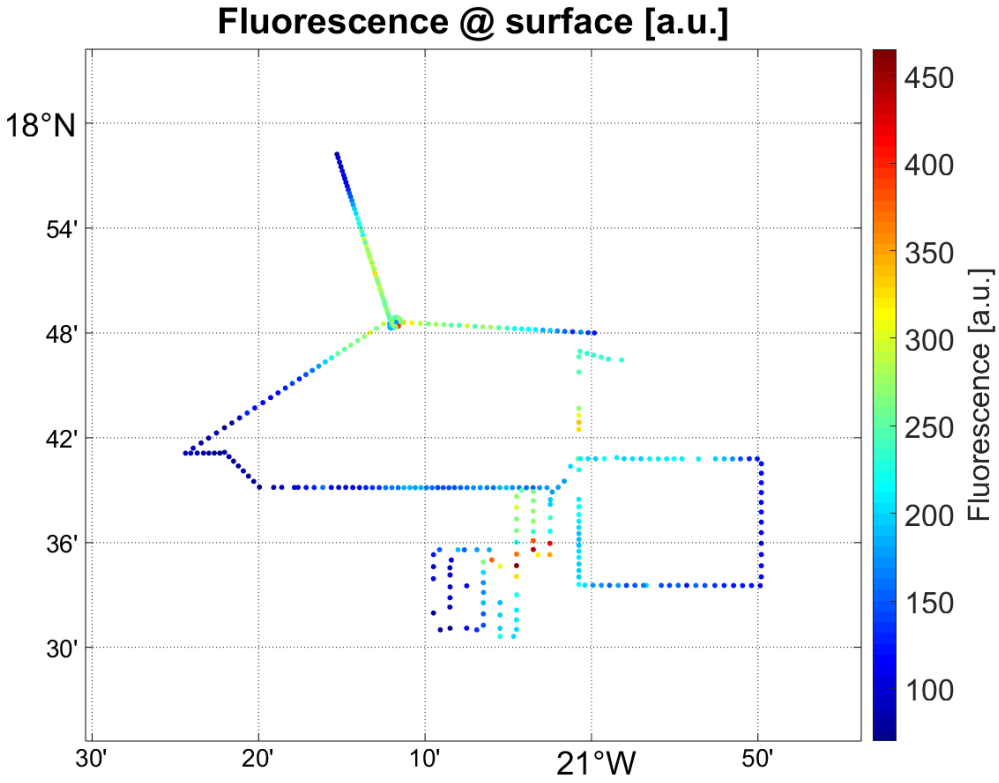


**Figure 5.2.6.3:** Example of raw fluorescence telemetry data of the SV3 Wave Glider inside and outside of the northeast cyclonic eddy studied during METEOR cruise M160.

### 5.2.7 Surface-Tethered Drifter Deployments

(N. Moradi[1], L. Hufnagel[1], G. Fischer[1], M. Iversen[1,2], C. Flintrop[2], M. Paulsen[3], B. Fiedler[3], A. Körtzinger[3])

[1]MARUM, [2]AWI, [3]GEOMAR

**Surface-tethered sediment trap drifters:** We deployed surface-tethered free-drifting sediment traps (from now on simply referred to as 'drifting traps'). The drifting trap array consisted of a top buoy with an attached Iridium satellite sender, an array of 14 2L-buoyancy spheres that acted as wave attenuation floats, two benthos spheres (glass floats) that provided 50 kg of buoyancy, and three trap stations each equipped with four gyroscopically mounted trap cylinders deployed at 100 m, 200 m, and 400 m, respectively (Fig. 5.2.7a-b). One trap cylinder per depth was fitted with a gel-filled collection cup to preserve the structure of the collected particles (Fig. 5.2.7c). The drifting traps collected sinking particles and marine aggregates at the three collection depths. The collected material was used to determine biogeochemical vertical flux, including total mass flux, particulate organic carbon, particulate organic nitrogen, particulate inorganic carbon, biogenic silica, and lithogenic material. The gel-filled collection cups collected intact, undisturbed aggregates, allowing determinations of the physical structure and size of the individual settling aggregates.

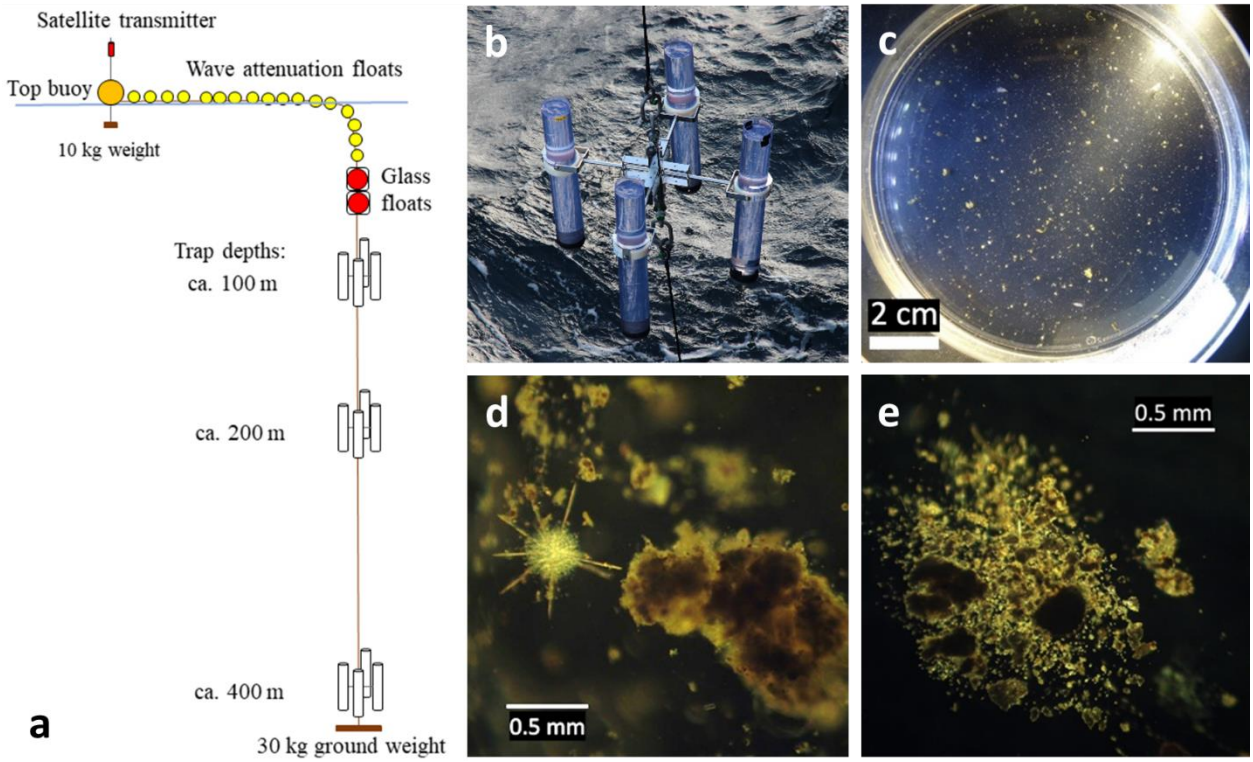


**Figure 5.2.7**: (a) Schematic drawing of the drifting sediment trap array used during M160. (b) A trap station with four trap cylinders mounted gyroscopically. (c) Example of a gel-filled collection cup recovered at 400 m (M160-170-1). (d)-(e) Microscope images of individual aggregates collected in the gel cup at 100 m (d) and 400 m (e).

A total of six deployments were carried out during the cruise; three in the first eddy, one outside the first eddy, and two in the second eddy (Table 5.2.7). Aggregates collected in the gel cups were imaged to analyze aggregate types and size-distribution at the respective depths (Fig. 5.2.7d-e). Material from one trap tube per depth was fixed with mercury chloride to determine the biogeochemical fluxes in the home laboratory. Samples for DNA sequencing and catalyzed reporter deposition fluorescence in situ hybridization (CARD-FISH) were taken from one of the other collection cylinders per depth. These samples as well as the collected material from the remaining biogeochemical collection cylinder were frozen at -20°C. The gel traps were imaged on board before those were frozen at -20°C. The gel traps will be imaged at high resolution in the home laboratory.

**BGC-Drifter:** Starting with station M160-87-1, a biogeochemical drifter (BGC) was also incorporated into the trap array at ca. 10 m depth below the glass floats. The BGC package consisted of a $CO_2$ sensor (HydroC CO2, CONTROS, Kiel, Germany, SN CO2-1117-001), an Oxygen Optode (Aanderaa Instruments AS, Bergen, Norway, SN ), a total gas tension sensor (HGTD, Pro-Oceanus Systems Inc., Halifax, Canada, SN ), a two channel fluorometer (FLNTURT, Sea-Bird Scientific, Bellevue, USA, SN ) during deployments 2 to 4 and a MicroFlu fluorometer (TriOS, Oldenburg, Germany, SN ) for deployments 5 and 6, a ProPS UV photometer (TriOS, Oldenburg, Germany, SN ) and a CTD (SBE 37, Sea-Bird Scientific, Bellevue, USA, SN 3411).

The BGC drifter is normally attached to a spar buoy for surface-tethered drift deployment as was planned to be deployed separately. During METEOR cruise M160, however, the two drifters

were combined into one drifting device to allow for better matching of the data and samples and save on deployment and recovery times for the instrument. This turned out to be a very effective decision. However, due to technical problems with one of the used data loggers some sensor data could not be fully recovered after deployments. This caused some gaps in obtained sensor data sets.

**Table 5.2.7**: List of sediment trap deployment and recovery times during METEOR cruise M160.

| Station | Date UTC | Time UTC | Action | Water depth (m) | Latitude (°) | Longitude (°) | Location/ Remark |
|---|---|---|---|---|---|---|---|
| M160-4-1 | 24/11/19 | 19:55 | Deployment | 4344 | 14° 30.014' N | 025° 10.108' W | Eddy 1 (center) |
| M160-12-1 | 25/11/19 | 19:25 | Recovery | 4294 | 14° 28.999' N | 025° 02.985' W | deployment 23.5 h |
| M160-87-1 | 02/12/19 | 23:22 | Deployment | 3168 | 17° 47.957' N | 020° 24.467' W | Eddy 2 (center) |
| M160-87-1* | 04/12/19 | 17:11 | Recovery | 3174 | 17° 44.549' N | 020° 30.826' W | deployment 42 h |
| M160-110-1 | 06/12/19 | 19:24 | Deployment | 3213 | 17° 48.500' N | 021° 14.334' W | Eddy 2 (west rim) |
| M160-16-1 | 07/12/19 | 17:42 | Recovery | 3225 | 17° 48.289' N | 021° 18.604' W | deployment 22.5 h |
| M160-146-1 | 12/12/19 | 20:50 | Deployment | 2395 | 14° 38.062' N | 024° 54.193' W | Eddy 1 (outside) |
| M160-164-1 | 13/12/19 | 20:50 | Recovery | 3647 | 14° 53.113' N | 024° 53.325' W | deployment 24.5 h |
| M160-170-1 | 14/12/19 | 10:03 | Deployment | 4408 | 14° 45.022' N | 025° 27.091' W | Eddy 1 (center) |
| M160-182-1 | 15/12/19 | 08:25 | Recovery | 4443 | 14° 40.136' N | 025° 31.882' W | deployment 22.5 h |
| M160-189-1 | 16/12/19 | 09:29 | Deployment | 4521 | 14° 37.512' N | 025° 48.536' W | Eddy 1 (south rim) |
| M160-198-1 | 17/12/19 | 13:17 | Recovery | 4591 | 14° 25.541' N | 025° 59.068' W | deployment 28 h |

## 5.3 Marine Ecology

### 5.3.1 Marine Protists Sampling

(S. Katzenmeier[1], M. Nothof[1], T. Stoeck[1])

[1]UNI-KL

During the M160 cruise our goal was to analyze the protistan community structure across vertical gradients of eddies as well as reference sites and to relate these structures to environmental variables. The second objective was to measure carbon fluxes mediated through microeukaryotic communities (top-down and bottom-up) and model the changes in protistan community structures and function (carbon turnover) based on predictions of alterations in the EBUS.

Water samples from three different depths were collected from CTD/RO casts at 14 stations. The deep chlorophyll maximum (DCM), the end of the photic zone (EPZ) and the oxygen minimum zone (OMZ) were the selected depths determined by the availability of auto-fluorescence and the oxygen concentration (Table 5.3.1).

**Table 5.3.1**: Stations and corresponding water depths from which water samples were taken for marine protist studies.

| Station | Latitude | Longitude | DCM (m) | EPZ (m) | OMZ (m) |
|---|---|---|---|---|---|
| M160-15-1 | 14° 28,999' N | 025° 02,985' W | 20 | 100 | 350 |
| M160-21-1 | 14° 29,664' N | 023° 32,081' W | 60 | 140 | 320 |
| M160-42-1 | 17° 12,711' N | 020° 36,279' W | 50 | 110 | 350 |
| M160-47-1 | 17° 36,766' N | 020° 36,052' W | 30 | 120 | 380 |
| M160-57-1 | 17° 49,084' N | 020° 36,051' W | 10 | 120 | 380 |
| M160-77-1 | 17° 48,728' N | 021° 12,494' W | 50 | 140 | 340 |

| | | | | | |
|---|---|---|---|---|---|
| M160-86-1 | 17° 48,542' N | 020° 48,012' W | 20 | 120 | 400 |
| M160-90-1 | 17° 48,881' N | 020° 24,542' W | 20 | 100 | 350 |
| M160-121-1 | 17° 35,432' N | 024° 16,957' W | 70 | 140 | 360 |
| M160-143-1 | 14° 36,511' N | 024° 54,783' W | 35 | 120 | 380 |
| M160-151-1 | 14° 36,967' N | 025° 03,888' W | 45 | 100 | 375 |
| M160-166-1 | 14° 26,134' N | 025° 14,933' W | 40 | 110 | 330 |
| M160-179-1 | 14° 43,270' N | 025° 29,374' W | 30 | 120 | 320 |
| M160-196-1 | 14° 18,382' N | 025° 14,384' W | 48 | 120 | 370 |

To analyze the carbon flux from bacteria to protists, short-term-grazing experiments were conducted based on the methodology developed by Hammer et al. (2001) and Gast et al. (2018). In detail, water samples taken from Niskin bottles were mixed with fluorescently labeled microspheres (10-15% of the concentration of the natural bacteria density in the sample). At the time points 0, 20, 45, and 90 min, subsamples were taken and immediately fixed using the Lugol's formalin technique. The preserved samples were applied to Isopore membrane filters (millipore) for subsequent epifluorescence microscopy. After staining the filters with DAPI (4',6-diamidin-2-phenylindole), the ingested food analogues ingested by protists can be counted. The following information can be obtained from the data: The specific feeding rate (prokaryotes/protist/h), the grazing effect (prokaryotes/mL/h), and the turnover of the daily carbon biomass, each for the entire protistan community and broken down by size fractions in the protist plankton (picozooplankton, nanozooplankton, microzooplankton). Each approach was carried out in triplicates for statistical validation.

To analyze shifts in the protistan plankton community, seawater was filtered on Durapore membranes (Millipore) immediately after sampling and conserved in a DNA stabilizing buffer until further processing in the laboratory. There, the nucleic acids are extracted and purified according to our standard protocols. The genomic environmental DNA obtained is amplified with protist-specific barcode primers via polymerase chain reaction (PCR), the sequencing banks are prepared and the amplified taxonomic DNA barcodes (V4 region of the gene of the small ribosomal subunit) are sequenced using the Illumina MiSeq platform (2x250 bp reads, paired-end). The bioinformatic analysis of the obtained genetic data includes the assembly of the individual reads, the elimination of sequences of insufficient quality, the clustering of the sequence data at species equivalence level and the taxonomic assignment of the data. Statistical analyses include classical methods for comparative analysis of biocoenosis (alpha, beta, and gamma diversity), spatial analysis methods (TAR, mantle), ordination analyses, and graph theory-based network analyses.

Through the assessment of the sequence data, we obtain the protistan community structure across vertical gradients of eddies and reference sites and can relate these structures to environmental variables. The evaluation of the experiments will allow us to better understand the carbon fluxes mediated through protistan communities. From the project we expect the first information on the influence of possible changes in the CanCS on protistan plankton community structure and function (photosynthetic fixation and export of carbon from the surface ocean; transfer of bacterial carbon to higher trophic levels) as a cornerstone and marker for ecosystem functioning and stability/resilience.

### 5.3.2 Zooplankton Sampling

(N. Moradi[1], L. Hufnagel[1], G. Fischer[1], M. Iversen[1,2], C. Flintrop[2], H. Hauss[3])

[1]MARUM, [2]AWI, [3]GEOMAR

Sinking marine aggregates play an important role in the ocean carbon cycle. The amount, sizes and sinking velocities of the aggregates determine how much carbon can be transported from the surface ocean to deep sea and sediments and, thus, determine the oceans' carbon sequestration. As the aggregates descend through the water column they are degraded by microbes and grazed on by zooplankton, which causes an attenuation of the export flux of organic carbon with increasing depth. During M160, we made direct on-board measurements of the microbial degradation using oxygen microsensors (see section 5.2.2) and can relate this to the amount flux attenuation determined by drifting traps and in situ camera systems. Typically, microbial degradation only accounts for a minor fraction of the upper ocean carbon flux attenuation and zooplankton grazing on settling aggregates seem to be the main attenuation mechanism in the upper few hundred meters of the water column (Iversen et al. 2010).

**Figure 5.3.2**: Preparation (left) and deployment (right) of the Hydrobios multinet with five nets for zooplankton sampling during METEOR cruise M160.

To estimate the role of zooplankton for flux attenuation we used a multinet (MSN, Hydrobios, Kiel) to quantify the vertical distribution of zooplankton types and abundance. The MSN was equipped with five nets of 200 µm mesh size (Fig. 5.3.2) and sampled mesozooplankton in five successive vertical layers in the water column (1000-600 m, 600-400 m, 400-200 m, 200-100 m and 100-0 m unless stated otherwise; Table 5.3.2). Time permitting, we did day and night hauls at the same station to account for diel vertical migration of zooplankton. In addition to sampling within the eddies, we carried out day and night hauls at the Cape Verde Ocean Observatory station to support the long-term zooplankton observation in the region (see Table 5.3.2). All zooplankton samples were fixed with 4% formaldehyde solution and stored at 4°C until analysis in the home laboratory. Combined with export flux measurements from drifting sediment traps (section 5.2.7) and camera profiles (section 5.2.4), the MSN samples will help us to identify potential effects of zooplankton spatial distribution and composition on carbon flux attenuation in cyclonic low oxygen eddies.

**Table 5.3.2**: List of multinet deployments during METEOR cruise M160.

| Station No. | Date (dd/mm/yy) | Time (hh:mm) | Water Depth (m) | Latitude (°) | Longitude (°) | Location |
|---|---|---|---|---|---|---|
| M160-16-1 | 25/11/19 | 22:48 | 4295 | 14° 28.998' N | 025° 02.985' W | Eddy 1 (center) |
| M160-48-1 | 30/11/19 | 14:19 | 3140 | 17° 47.963' N | 020° 36.023' W | Eddy 2 (center) |
| M160-58-1 | 01/12/19 | 00:26 | 3136 | 17° 49.086' N | 020° 36.049' W | Eddy 2 (center) |
| M160-93-1 | 03/12/19 | 04:26 | 3155 | 17° 48.881' N | 020° 24.542' W | Eddy 2 (center) |
| M160-108-1 | 06/12/19 | 16:31 | 3223 | 17° 47.450' N | 021° 13.177' W | Eddy 2 (west rim) |
| M160-114-1 | 06/12/19 | 21:41 | 3201 | 17° 49.834' N | 021° 14.414' W | Eddy 2 (west rim) |
| M160-118-1 | 09/12/19 | 05:55 | 3611 | 17° 34.963' N | 024° 16.978' W | CVOO |
| M160-122-1 | 09/12/19 | 12:18 | 3614 | 17° 35.431' N | 024° 16.955' W | CVOO (600 m profile) |
| M160-140-1 | 12/12/19 | 14:041 | 2900 | 14° 36.295' N | 024° 54.896' W | Eddy 1 (outside) |
| M160-147-1 | 12/12/19 | 21:59 | 2662 | 14° 36.643' N | 024° 54.846' W | Eddy 1 (outside) |
| M160-174-1 | 15/12/19 | 00:05 | 4423 | 14° 42.701' N | 025° 29.487' W | Eddy 1 (center) |
| M160-183-1 | 16/12/19 | 04:22 | 4496 | 14° 39.538' N | 025° 45.445' W | Eddy 1 (south rim) |
| M160 190-1 | 16/12/19 | 10:16 | 4522 | 14° 37.960' N | 025° 49.039' W | Eddy 1 (south rim) |

## 5.4 Remote Sensing of Ocean Color

M. Hieronymi[1], R. Röttgers[1], D. Behr[1], H. Krasemann[1], K. Heymann[1], K. Becker[2], Q. Devresse[2])

[1]HZG, [2]GEOMAR

Satellite remote sensing of ocean color provides global monitoring of the marine biomass and other water constituents. It is particularly suited for large-scale and near-real time observations of the region of interest. In this study around the Cape Verde islands, starting months before and during the M160 cruise, ocean color data supported the detection of suitable eddies and frontal systems.

Objectives of the campaign were to measure the hyperspectral remote-sensing reflectance (ocean color) and radiance distribution of sun and sky light as well as to determine constituents of water samples from the upper ocean mixed layer. The overall goal of the work is to validate and improve ocean color algorithms, in particular the Sentinel-3/OLCI Neural Network Swarm (ONNS) algorithm (Hieronymi et al. 2017), and their atmospheric corrections by means of satellite match-ups. Beyond Sentinel-3/OLCI, also other operational satellite sensors were of interest (Sentinel-2/MSI, Aqua/MODIS, VIIRS, ISS/DESIS) in order to validate atmospheric corrections and band-shifting procedures (Hieronymi, 2019). As a supplement to the MOSES Eddy Study II, another aim of the campaign was to obtain simultaneous reflectance measurements at sea and from the motor-glider STEMME, mainly in view of the ground-truthing of the airborne HySpex (NEO, Norway) imagery, and if possible to monitor gradients of ocean color along frontal systems. Moreover, specific questions of the solar radiative transfer at the wavy air-sea interface were subject of investigation (see Hieronymi (2016)).

The radiative budget at the sea surface was investigated during daylight stations of RV METEOR and partly during frontal transects of the slow-moving vessel. Hyperspectral (350 to 950 nm) Ramses sensors by TriOS GmbH (Germany) were used to measure:

- downwelling irradiance at the sea surface, $E_d^+(\lambda)$,
- sky radiance with different sun-viewing angles, $L_{sky}(\lambda,\theta,\varphi)$, and
- upwelling radiance from the sea surface, $L_{surf}(\lambda,\theta',\varphi)$.

Remote-sensing reflectance,$R_{rs}$, is determined from these three quantities (Ruddick et al. 2019a+b). Furthermore, a hyperspectral (450 to 950 nm) camera by Cubert GmbH (Germany) was utilized for the first time at sea to characterize the full radiance distribution of the sky and of the surface-reflected light, i.e. $L_{sky}(\lambda,\theta,\varphi)$ and $L_{surf}(\lambda,\theta',\varphi)$.

In addition to that, water samples from the upper ocean mixed layer were collected during CTD/RO casts by the GEOMAR team (K. Becker, Q. Devresse); this sampling did not necessarily coincide with the reflectance measurements. The water samples from different water depths were filtered on board. The GF/F filters were shock-frozen for later HPLC pigment analysis in the HZG lab, i.e. determination of the chlorophyll content and other parameters. Filtered water samples were cool-stored for later analysis at GEOMAR and after that in the HZG lab for determination of the spectral CDOM absorption (colored dissolved organic matter). In summary:

- In total, 40 units of hyperspectral remote-sensing reflectance measurements were conducted (with data acquisition times between 10 min and 5 h); thereof 14 units with coinciding characterization of the full sky-surface radiance distribution.
- Approximately nine of these data acquisitions where conducted during slow-moving transects across different water masses.
- Different coincident measurements with STEMME overflights from different directions were realized. Beyond reflectance, DSHIP water temperature was also determined in situ for comparison with airborne remote sensing data.
- Valuable clear sky match-ups with satellite overflights were obtained, including Sentinel-3A/OLCI, Sentinel-3B/OLCI, Aqua/MODIS and VIIRS.

## 5.5 Atmospheric Aerosol Sampling

(K.W. Fomba[1], B. Fiedler[2])

[1]TROPOS, [2]GEOMAR

Aerosol sampling was performed during the M160 Cruise to characterize the impact of eddies on the flux of nitrate and other enriched chemical compounds at the surface waters to the atmosphere. Due to the different sampling locations, a broader spatial coverage could be achieved providing a better overview of the effects of different oceanic processes and regions on the atmospheric composition. Total suspended aerosol particles were collected on quartz fiber filters using a filter holder system connected to a low volume membrane vacuum pump (ABM, Marktredwitz, Germany) operating at a flow rate of 2 $m^3\ h^{-1}$ (Fig. 5.5.1). The filter holder sampling system was attached to the railing of the deck of RV METROR above the chemistry laboratory about 3 m above the bearing deck. The sampling height was about 18 m above sea level. Samples were collected on a daily routine from 24/11/2019 to 18/12/2019 during the cruise. After sampling, the samples were frozen to prevent the loss of volatile organic species due to ambient temperature variation.

In total, 21 samples were collected. The samples will be analyzed for their chemical composition, especially their nitrogen and phosphate content. This includes the water-soluble organic nitrate, and total nitrate content using ion chromatographic and thermo-catalytic oxidation approach (Fomba et al. 2014). In addition, the organic and elemental carbon contents of the samples will be analyzed using thermo-optical methods to investigate the role of long-range transport on the local atmospheric composition. By applying different transport parametrizations,

the flux of the chemical species from the surface waters to the atmosphere during the dynamics of the eddies will be estimated. The detailed analysis will provide information about the changes in the atmospheric chemical composition along different tracks and regions in the Atlantic during the dynamics of the eddies. The results would help to elucidate the role of eddies on the temporal and seasonal variation in time-series observations of marine atmospheric budgets of nitrogen compounds and aerosol chemical constituents in the eastern tropical Atlantic region.

**Figure 5.5:** Picture of the aerosol filter holder sampling system (left) and samples collected during the M160 cruise (right) with brown colored filters indicating samples influenced by Saharan dust.

## 5.6 Airborne Measurement Program (Research Motorglider STEMME)

(B. Baschek[1], R. Röttgers[1])

[1]HZG

Part of research cruise M160 were aerial surveys with research motorglider STEMME of the University of Applied Sciences Aachen. The measurements were carried out by HZG and contained very high-resolution measurements of the sea surface with infrared and hyperspectral cameras.

The camera systems were installed in the wing pods of the plane and were looking straight down onto the sea surface. Combined with an IMU with < 0.2° resolution, maps of sea surface temperature (5 m horizontal and 0.03 K temperature resolution) and ocean color (3 m horizontal resolution) were generated. The data were transmitted in real time to RV METEOR over a distance of up to 80 km and to a land station that was based on the island of Sal. The aerial data were used to locate the exact position of the mesoscale eddies, provide a spatial overview of (parts of) the observed mesoscale eddies and for detailed observations of smaller-scale processes at their flanks. Special focus was given to on quickly evolving sub-mesoscale instabilities at the frontal region of the mesoscale eddies.

During the cruise, a total of 11 measurement flights were carried out and exemplary data are shown in Fig. 5.6.1.


**Figure 5.6.1**: Chief pilot Philipp Hilker and Prof. Burkard Baschek before departure of motorglider STEMME (left) and overflight of RV METEOR as seen from the plane (middle) and from the vessel (right).

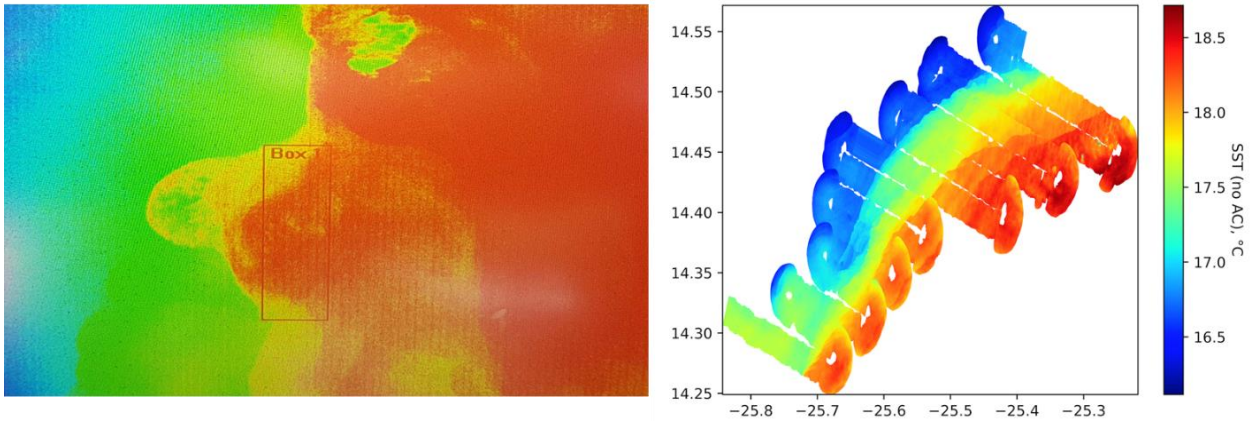


**Figure 5.6.2**: Sea surface temperature maps of a single video frame showing small-scale structure on the scale of approximately 500 m (left) and a composite map of an entire flight (right), both taken on 12/12/2019 at the southeastern edge of the mesoscale eddy that was located to the southwest of the island of Fogo.

## 6 Ship's Meteorological Station

(A. Raeke[1])

[1]DWD

RV METEOR departed from the port of Mindelo/Cabo Verde in the morning of 23/11/2019 under a clear sky and a northeastern trade wind 3-4 Bft. Under influence of the Azores high, the general weather situation was determined by northeastern trade winds with 5-6 Bft and a significant wave height of mostly 1.5-2.5 m. Throughout the cruise, luv and lee effects as land/sea breezes and katabatic winds were encountered around some Cabo Verdean islands. Between the islands São Vicente and Santo Antão, on the way to the first research area, there was immediately a luv effect with winds of 6 Bft. In the leeward area of the islands, the northeasterly wind decreased briefly to 4 Bft. On 24/11/2019, Cabe Verde was located just south of a subtropical high ridge. In the following night, the research work began southwest of Fogo with a steady northeast trade wind of 5 Bft and a significant wave height of 2-2.5 m. Depending on the location of RV METEOR relative to the island of Fogo, wind varied on 25/11/2019 at 2-6 Bft.

On 26/11 to 27/11/2019, during transit to the second research area northeast of Sal, strong luv and lee effects could be observed again between the islands Fogo and Santiago. Afterwards weather conditions continued with a moderate northeast trade wind of about 5 Bft and a significant wave height of approximately 2 m. From the 28/11/2019 to 02/12/2019, due to a weakening Azores high, good working conditions prevailed for zodiac operations with a trade wind of approx. 4 Bft and a significant wave height of 1-1.5 m. Starting from 03/12/2019, trade wind intensified between a strengthening Azores high and a low close to Morocco. Winds blew from now on with 6 Bft until the morning of 06/12/2019 when the Azores high lost its influence and a cold front of the low near Morocco passed RV METEOR with light showers. The wind decreased for a short period to 4-5 Bft. On the backside of the cold front, wind increased again to 6 Bft.

In the following days, the high pressure influence over the North Atlantic increased again (Azores high 1045 hPa on 11/12/2019). From the Sahara now increasingly extensive dusty air was introduced, which reduced visibility to less than 10 km and lead to dry deposition of mineral dust on the deck of RV METEOR. With a significant wave height of 2-3 m and wind of 6-7 Bft, the recovery of the scientific equipment was postponed by one day to the 10/12/2019 in order to take advantage of the predicted short-term decreases in wind and wind sea working area.

On 11/12/2019, the return to the research area southwest of the Fogo took place with a tail wind of mostly 6 Bft and a significant wave height of 2 m. In the morning hours of 12/12/2019, 6-7 Bft were reached by the luv effect, whereas in lee of Fogo it was almost calm again. Only on 14/12 to 15/12/2019, trade wind weakened temporarily to 4 Bft. The Azores high was disturbed by a shifting front. The significant wave height decreased to 1.5-2 m. On 16/12/2019, the Azores high increased temporarily again and the wind increased to 6-7 Bft. In connection with an incoming higher swell of 3 m height, a significant wave height of 3.5 m was reached during the last days of research. The last scientific devices were therefore recovered on 18/12/2019, when as predicted wind decreased to 5-6 Bft on 18/12/2019. On 18/12 to 19/12/2019, during transit from Fogo to southwest of Santo Antão (Tarrafal) the trade wind blew with 5-6 Bft and high swell of 2.5-3 m on the open sea remained. Finally, weak winds were encountered as planned in lee of Santo Antao (Bay of Tarrafal), where the rendezvous with RV MARIA S. MERIAN took place and the container packing started at sea already.

# 7 Station List M160

| Station | Date in 2019 | Time [UTC] | Device | Latitude | Longitude | Water Depth (m) | Remarks |
|---|---|---|---|---|---|---|---|
| M160-1-1 | 24/11 | 09:56 | GLD/D | 14° 30,028' N | 026° 00,029' W | 4581 | |
| M160-2-1 | 24/11 | 10:49 | WGLD/D | 14° 30,025' N | 026° 00,030' W | 4580 | |
| M160-3-1 | 24/11 | 11:34 | GLD/D | 14° 30,049' N | 026° 00,044' W | 4580 | |
| M160-4-1 | 24/11 | 19:56 | DST/D | 14° 30,014' N | 025° 10,108' W | 4344 | |
| M160-5-1 | 24/11 | 20:54 | CTD/RO 01 | 14° 30,204' N | 025° 10,169' W | 4346 | Profile depth 2000 m |
| M160-6-1 | 24/11 | 23:25 | MSS 01 | 14° 31,914' N | 025° 10,410' W | 4360 | |
| M160-7-1 | 24/11 | 23:32 | FLOAT | 14° 32,119' N | 025° 10,384' W | 4354 | Argo Float |
| M160-8-1 | 24/11 | 23:37 | FLOAT | 14° 32,306' N | 025° 10,358' W | 4348 | BGC-Argo Float |
| M160-9-1 | 24/11 | 23:40 | SVP | 14° 32,390' N | 025° 10,355' W | 4344 | |
| M160-10-1 | 25/11 | 12:25 | CTD/RO 02 | 14° 30,059' N | 024° 59,923' W | 4196 | Full depth profile |
| M160-11-1 | 25/11 | 18:43 | MOOR/D | 14° 32,786' N | 025° 00,166' W | 4017 | KPO 1217 |
| M160-12-1 | 25/11 | 20:03 | DST/R | 14° 28,999' N | 025° 02,985' W | 4294 | |
| M160-13-1 | 25/11 | 20:25 | MSC | 14° 28,999' N | 025° 02,986' W | 4297 | Sampling depth 20 m |
| M160-14-1 | 25/11 | 20:36 | MSC | 14° 29,000' N | 025° 02,984' W | 4292 | Sampling depth 17 m |
| M160-15-1 | 25/11 | 21:23 | CTD/RO 03 | 14° 28,999' N | 025° 02,985' W | 4297 | Profile depth 1000 m |
| M160-16-1 | 25/11 | 22:48 | MSN | 14° 28,998' N | 025° 02,985' W | 4295 | Profile depth 1000 m |
| M160-17-1 | 26/11 | 15:40 | CTD/RO 04 | 14° 29,962' N | 023° 33,029' W | 3939 | Profile depth 2000 m |
| M160-18-1 | 26/11 | 17:06 | GLD/D | 14° 29,960' N | 023° 33,029' W | 3941 | |
| M160-19-1 | 26/11 | 17:23 | GLD/D | 14° 29,957' N | 023° 33,030' W | 3943 | |
| M160-20-1 | 26/11 | 19:08 | MSS 02 | 14° 29,673' N | 023° 32,092' W | 3940 | |
| M160-21-1 | 26/11 | 19:32 | CTD/RO 05 | 14° 29,664' N | 023° 32,081' W | 3939 | Profile depth 500 m |
| M160-22-1 | 26/11 | 19:57 | FLOAT | 14° 29,641' N | 023° 32,018' W | 3937 | Argo Float |
| M160-23-1 | 26/11 | 19:58 | SVP | 14° 29,640' N | 023° 31,991' W | 3937 | |
| M160-24-1 | 27/11 | 12:16 | CTD/RO 06 | 16° 00,065' N | 021° 59,966' W | 3432 | Profile depth 1200 m |
| M160-25-1 | 27/11 | 15:33 | CTD/RO 07 | 16° 20,122' N | 022° 00,019' W | 3619 | Profile depth 1200 m |
| M160-26-1 | 27/11 | 18:53 | CTD/RO 08 | 16° 39,994' N | 021° 59,984' W | 3525 | Profile depth 1200 m |
| M160-27-1 | 27/11 | 22:11 | CTD/RO 09 | 17° 00,093' N | 021° 59,962' W | 3384 | Profile depth 1200 m |
| M160-28-1 | 28/11 | 00:26 | CTD/RO 10 | 17° 11,263' N | 021° 57,116' W | 110 | Profile depth 100 m |
| M160-29-1 | 28/11 | 02:16 | CTD/RO 11 | 17° 20,028' N | 021° 59,974' W | 3029 | Profile depth 1200 m |
| M160-30-1 | 28/11 | 05:36 | CTD/RO 12 | 17° 41,542' N | 021° 59,983' W | 3340 | Profile depth 1200 m |
| M160-31-1 | 28/11 | 07:50 | CTD/RO 13 | 17° 50,007' N | 021° 59,995' W | 3322 | Profile depth 1200 m |
| M160-32-1 | 28/11 | 10:09 | CTD/RO 14 | 18° 00,059' N | 022° 00,026' W | 3305 | Profile depth 1200 m |
| M160-33-1 | 28/11 | 12:30 | CTD/RO 15 | 18° 10,085' N | 022° 00,012' W | 3308 | Profile depth 1200 m |
| M160-34-1 | 28/11 | 14:47 | CTD/RO 16 | 18° 20,031' N | 022° 00,027' W | 3321 | Profile depth 1200 m |
| M160-35-1 | 28/11 | 17:10 | CTD/RO 17 | 18° 30,017' N | 021° 59,998' W | 3333 | Profile depth 1200 m |
| M160-36-1 | 28/11 | 22:48 | CTD/RO 18 | 18° 00,049' N | 022° 29,997' W | 3338 | Profile depth 1200 m |
| M160-37-1 | 29/11 | 01:34 | CTD/RO 19 | 17° 59,954' N | 022° 14,920' W | 3322 | Profile depth 1200 m |
| M160-38-1 | 29/11 | 22:46 | CTD/RO 20 | 17° 00,001' N | 020° 36,002' W | 3438 | Profile depth 1200 m |
| M160-39-1 | 30/11 | 00:22 | MSS 03 | 17° 00,330' N | 020° 36,475' W | 3440 | |
| M160-40-1 | 30/11 | 02:08 | CTD/RO 21 | 17° 12,006' N | 020° 35,955' W | 3396 | Profile depth 1200 m |
| M160-41-1 | 30/11 | 03:50 | MSS 04 | 17° 12,682' N | 020° 36,269' W | 3394 | |
| M160-42-1 | 30/11 | 04:18 | CTD/RO 22 | 17° 12,711' N | 020° 36,279' W | 3393 | Profile depth 500 m |
| M160-43-1 | 30/11 | 06:37 | CTD/RO 23 | 17° 23,990' N | 020° 35,956' W | 3327 | Profile depth 1200 m |
| M160-44-1 | 30/11 | 08:20 | MSS 05 | 17° 24,399' N | 020° 35,799' W | 3327 | |
| M160-45-1 | 30/11 | 10:04 | CTD/RO 24 | 17° 36,005' N | 020° 35,997' W | 3226 | Profile depth 1200 m |
| M160-46-1 | 30/11 | 11:48 | MSS 06 | 17° 36,746' N | 020° 36,055' W | 3216 | |
| M160-47-1 | 30/11 | 12:16 | CTD/RO 25 | 17° 36,766' N | 020° 36,052' W | 3220 | Profile depth 500 m |
| M160-48-1 | 30/11 | 14:19 | MSN | 17° 47,963' N | 020° 36,023' W | 3140 | Profile depth 1000 m |
| M160-49-1 | 30/11 | 15:39 | CTD/RO 26 | 17° 47,964' N | 020° 36,026' W | 3139 | Profile depth 800 m |
| M160-50-1 | 30/11 | 16:35 | GLD/D | 17° 47,960' N | 020° 36,020' W | 3139 | |
| M160-51-1 | 30/11 | 17:08 | GLD/D | 17° 47,959' N | 020° 36,020' W | 3140 | |
| M160-52-1 | 30/11 | 17:52 | GLD/D | 17° 47,960' N | 020° 36,021' W | 3141 | |
| M160-53-1 | 30/11 | 18:55 | MSC | 17° 47,962' N | 020° 36,022' W | 3139 | Sampling depth 34 m |
| M160-54-1 | 30/11 | 19:07 | MSC | 17° 47,963' N | 020° 36,024' W | 3139 | Sampling depth 40 m |
| M160-55-1 | 30/11 | 20:10 | CTD/RO 27 | 17° 47,961' N | 020° 36,022' W | 3140 | Profile depth 1200 m |
| M160-56-1 | 30/11 | 22:38 | MSS 07 | 17° 49,075' N | 020° 36,044' W | 3138 | |
| M160-57-1 | 30/11 | 23:21 | CTD/RO 28 | 17° 49,084' N | 020° 36,051' W | 3136 | Profile depth 1000 m |
| M160-58-1 | 01/12 | 00:26 | MSN | 17° 49,086' N | 020° 36,049' W | 3136 | Profile depth 1000 m |
| M160-59-1 | 01/12 | 01:16 | FLOAT | 17° 49,162' N | 020° 36,155' W | 3135 | BGC-Argo Float |
| M160-60-1 | 01/12 | 01:22 | FLOAT | 17° 49,365' N | 020° 36,269' W | 3135 | BGC-Argo Float |
| M160-61-1 | 01/12 | 01:26 | FLOAT | 17° 49,462' N | 020° 36,327' W | 3132 | Argo Float |
| M160-62-1 | 01/12 | 01:27 | SVP | 17° 49,505' N | 020° 36,353' W | 3133 | |

| | | | | | | | |
|---|---|---|---|---|---|---|---|
| M160-63-1 | 01/12 | 03:08 | CTD/RO 29 | 18° 00,030' N | 020° 36,011' W | 3091 | Profile depth 1200 m |
| M160-64-1 | 01/12 | 04:56 | MSS 08 | 18° 00,785' N | 020° 36,262' W | 3086 | |
| M160-65-1 | 01/12 | 06:38 | CTD/RO 30 | 18° 11,977' N | 020° 36,036' W | 3125 | Profile depth 1200 m |
| M160-66-1 | 01/12 | 08:23 | MSS 09 | 18° 12,342' N | 020° 36,628' W | 3126 | |
| M160-67-1 | 01/12 | 10:08 | CTD/RO 31 | 18° 24,021' N | 020° 36,021' W | 3175 | Profile depth 1200 m |
| M160-68-1 | 01/12 | 11:21 | MSS 10 | 18° 24,042' N | 020° 36,035' W | 3177 | |
| M160-69-1 | 01/12 | 13:43 | CTD/RO 32 | 18° 35,999' N | 020° 36,026' W | 3212 | Profile depth 1200 m |
| M160-70-1 | 01/12 | 15:39 | MSS 11 | 18° 36,576' N | 020° 36,390' W | 3212 | |
| M160-71-1 | 01/12 | 15:51 | MSC | 18° 36,579' N | 020° 36,399' W | 3212 | Sampling depth 40 m |
| M160-72-1 | 01/12 | 16:05 | MSC | 18° 36,579' N | 020° 36,400' W | 3212 | Sampling depth 40 m |
| M160-73-1 | 02/12 | 02:26 | CTD/RO 33 | 17° 48,053' N | 021° 24,026' W | 3239 | Profile depth 1200 m |
| M160-74-1 | 02/12 | 04:07 | MSS 12 | 17° 48,698' N | 021° 24,382' W | 3236 | |
| M160-75-1 | 02/12 | 06:15 | CTD/RO 34 | 17° 48,071' N | 021° 12,081' W | 3205 | Profile depth 1200 m |
| M160-76-1 | 02/12 | 08:07 | MSS 13 | 17° 48,710' N | 021° 12,488' W | 3203 | |
| M160-77-1 | 02/12 | 08:37 | CTD/RO 35 | 17° 48,728' N | 021° 12,494' W | 3203 | Profile depth 500 m |
| M160-78-1 | 02/12 | 09:38 | WGLD/R | 17° 49,227' N | 021° 11,463' W | 3197 | |
| M160-79-1 | 02/12 | 10:12 | GLD/D | 17° 49,195' N | 021° 11,437' W | 3195 | |
| M160-80-1 | 02/12 | 10:42 | GLD/D | 17° 49,170' N | 021° 11,419' W | 3197 | |
| M160-81-1 | 02/12 | 13:28 | CTD/RO 36 | 17° 47,934' N | 021° 00,062' W | 3162 | Profile depth 1200 m |
| M160-82-1 | 02/12 | 15:29 | MSS 14 | 17° 48,353' N | 021° 00,324' W | 3157 | |
| M160-83-1 | 02/12 | 15:42 | WGLD/D | 17° 48,287' N | 021° 00,394' W | 3158 | |
| M160-84-1 | 02/12 | 17:50 | CTD/RO 37 | 17° 47,992' N | 020° 48,075' W | 3134 | Profile depth 800 m |
| M160-85-1 | 02/12 | 19:24 | MSS 15 | 17° 48,538' N | 020° 48,010' W | 3130 | |
| M160-86-1 | 02/12 | 19:58 | CTD/RO 38 | 17° 48,542' N | 020° 48,012' W | 3131 | Profile depth 500 m |
| M160-87-1 | 02/12 | 23:28 | DST/D | 17° 47,957' N | 020° 24,467' W | 3168 | With BGC drifter |
| M160-88-1 | 03/12 | 00:30 | CTD/RO 39 | 17° 48,382' N | 020° 24,456' W | 3160 | Profile depth 1200 m |
| M160-89-1 | 03/12 | 02:12 | MSS 16 | 17° 48,881' N | 020° 24,541' W | 3154 | |
| M160-90-1 | 03/12 | 02:44 | CTD/RO 40 | 17° 48,881' N | 020° 24,542' W | 3155 | Profile depth 500 m |
| M160-91-1 | 03/12 | 03:17 | MSC | 17° 48,880' N | 020° 24,541' W | 3154 | Sampling depth 60 m |
| M160-92-1 | 03/12 | 03:29 | MSC | 17° 48,880' N | 020° 24,542' W | 3155 | Sampling depth 60 m |
| M160-93-1 | 03/12 | 04:26 | MSN | 17° 48,881' N | 020° 24,542' W | 3155 | Profile depth 1000 m |
| M160-94-1 | 03/12 | 06:59 | CTD/RO 41 | 17° 48,000' N | 020° 12,022' W | 3199 | Profile depth 1200 m |
| M160-95-1 | 03/12 | 08:33 | MS2 17 | 17° 48,729' N | 020° 11,961' W | 3198 | |
| M160-96-1 | 03/12 | 10:16 | CTD/RO 42 | 17° 48,007' N | 019° 59,997' W | 3239 | Profile depth 1200 m |
| M160-97-1 | 03/12 | 12:06 | MSS 18 | 17° 48,384' N | 019° 59,890' W | 3236 | |
| M160-98-1 | 03/12 | 14:35 | CTD/RO 43 | 17° 47,941' N | 019° 42,022' W | 3262 | Profile depth 1200 m |
| M160-99-1 | 03/12 | 16:48 | MSS 19 | 17° 48,140' N | 019° 41,746' W | 3264 | |
| M160-87-1 | 04/12 | 17:46 | DST/R | 17° 44,549' N | 020° 30,826' W | 3174 | |
| M160-100-1 | 04/12 | 18:32 | CTD/RO 44 | 17° 44,973' N | 020° 30,889' W | 3169 | Profile depth 600 m |
| M160-101-1 | 05/12 | 13:36 | DCTD | 17° 39,969' N | 021° 04,885' W | 3243 | Start of dye release |
| M160-101-1 | 05/12 | 14:23 | DCTD | 17° 39,701' N | 021° 05,878' W | 3244 | End of dye release |
| M160-102-1 | 05/12 | 13:36 | SVP | 17° 39,969' N | 021° 05,867' W | 3243 | Modified SVP drifter |
| M160-103-1 | 05/12 | 14:22 | SVP | 17° 39,703' N | 021° 07,026' W | 3245 | Modified SVP drifter |
| M160-104-1 | 05/12 | 23:40 | CTD/RO 45 | 17° 40,918' N | 021° 05,550' W | 3234 | Profile depth 500 m |
| M160-105-1 | 06/12 | 00:40 | CTD/RO 46 | 17° 43,465' N | 021° 05,399' W | 3223 | Profile depth 500 m |
| M160-106-1 | 06/12 | 04:57 | CTD/RO 47 | 17° 48,003' N | 020° 24,234' W | 3170 | Profile depth 100 m |
| M160-107-1 | 06/12 | 10:01 | GLD/R | 17° 37,195' N | 021° 03,960' W | 3263 | |
| M160-108-1 | 06/12 | 16:31 | MSN | 17° 47,450' N | 021° 13,177' W | 3223 | Profile depth 1000 m |
| M160-109-1 | 06/12 | 17:52 | CTD/RO 48 | 17° 47,973' N | 021° 14,002' W | 3216 | Profile depth 1200 m |
| M160-110-1 | 06/12 | 19:25 | DST/D | 17° 48,500' N | 021° 14,334' W | 3213 | With BGC drifter |
| M160-111-1 | 06/12 | 20:22 | MSS 20 | 17° 49,281' N | 021° 14,117' W | 3205 | |
| M160-112-1 | 06/12 | 20:41 | MSC | 17° 49,327' N | 021° 14,191' W | 3204 | Sampling depth 60 m |
| M160-113-1 | 06/12 | 20:57 | MSC | 17° 49,413' N | 021° 14,380' W | 3204 | Sampling depth 60 m |
| M160-114-1 | 06/12 | 21:41 | MSN | 17° 49,834' N | 021° 14,414' W | 3201 | Profile depth 1000 m |
| M160-115-1 | 06/12 | 23:06 | CTD/RO 49 | 17° 49,982' N | 021° 14,370' W | 3199 | Profile depth 1200 m |
| M160-116-1 | 07/12 | 18:14 | DST/R | 17° 48,289' N | 021° 18,604' W | 3225 | |
| M160-117-1 | 07/12 | 19:47 | CTD/RO 50 | 17° 49,183' N | 021° 19,723' W | 3227 | Profile depth 1200 m |
| M160-118-1 | 09/12 | 05:55 | MSN | 17° 34,963' N | 024° 16,978' W | 3611 | Profile depth 1000 m |
| M160-119-1 | 09/12 | 08:02 | CTD/RO 51 | 17° 35,001' N | 024° 17,012' W | 3611 | Full depth profile |
| M160-120-1 | 09/12 | 10:40 | MSS 21 | 17° 35,417' N | 024° 16,948' W | 3613 | |
| M160-121-1 | 09/12 | 11:35 | CTD/RO 52 | 17° 35,432' N | 024° 16,957' W | 3615 | Profile depth 500 m |
| M160-122-1 | 09/12 | 12:18 | MSN | 17° 35,431' N | 024° 16,955' W | 3614 | Profile depth 600 m |
| M160-123-1 | 09/12 | 12:50 | FLOAT | 17° 35,500' N | 024° 16,983' W | 3614 | Argo Float |
| M160-124-1 | 09/12 | 12:52 | SVP | 17° 35,580' N | 024° 16,885' W | 3615 | |
| M160-125-1 | 10/12 | 08:13 | GLD/R | 17° 48,235' N | 022° 27,815' W | 3339 | |
| M160-126-1 | 10/12 | 16:05 | GLD/R | 17° 34,188' N | 021° 08,498' W | 3304 | |
| M160-127-1 | 10/12 | 16:28 | GLD/R | 17° 34,368' N | 021° 08,450' W | 3300 | |

| | | | | | | | |
|---|---|---|---|---|---|---|---|
| M160-128-1 | 10/12 | 16:50 | GLD/R | 17° 34,883' N | 021° 08,267' W | 3292 | |
| M160-129-1 | 10/12 | 17:24 | GLD/R | 17° 35,927' N | 021° 07,857' W | 3281 | |
| M160-130-1 | 10/12 | 18:00 | GLD/R | 17° 34,748' N | 021° 08,454' W | 3294 | |
| M160-131-1 | 10/12 | 19:07 | WGLD/R | 17° 37,253' N | 021° 05,360' W | 3264 | |
| M160-132-1 | 12/12 | 00:33 | CTD/RO 53 | 15° 05,996' N | 025° 15,107' W | 4305 | Profile depth 1200 m |
| M160-133-1 | 12/12 | 01:52 | MSS 22 | 15° 06,182' N | 025° 15,438' W | 4284 | |
| M160-134-1 | 12/12 | 03:29 | CTD/RO 54 | 14° 55,860' N | 025° 15,025' W | 4291 | Profile depth 1200 m |
| M160-135-1 | 12/12 | 05:08 | MSS 23 | 14° 55,856' N | 025° 14,944' W | 4288 | |
| M160-136-1 | 12/12 | 06:44 | CTD/RO 55 | 14° 46,059' N | 025° 15,083' W | 4315 | Profile depth 1200 m |
| M160-137-1 | 12/12 | 08:25 | MSS 24 | 14° 47,111' N | 025° 14,787' W | 4309 | |
| M160-138-1 | 12/12 | 08:38 | WGLD/D | 14° 47,134' N | 025° 14,877' W | 4307 | |
| M160-139-1 | 12/12 | 11:30 | GLD/R | 14° 55,859' N | 025° 03,125' W | 4171 | |
| M160-140-1 | 12/12 | 14:41 | MSN | 14° 36,295' N | 024° 54,896' W | 2900 | Profile depth 1000 m |
| M160-141-1 | 12/12 | 16:01 | CTD/RO 56 | 14° 36,881' N | 024° 54,594' W | 2560 | Profile depth 1200 m |
| M160-142-1 | 12/12 | 16:58 | MSS 25 | 14° 37,382' N | 024° 54,655' W | 2435 | |
| M160-143-1 | 12/12 | 19:01 | CTD/RO 57 | 14° 36,511' N | 024° 54,783' W | 2701 | Profile depth 500 m |
| M160-144-1 | 12/12 | 19:42 | MSC | 14° 37,313' N | 024° 54,459' W | 2516 | Sampling depth 42 m |
| M160-145-1 | 12/12 | 19:55 | MSC | 14° 37,576' N | 024° 54,364' W | 2501 | Sampling depth 57 m |
| M160-146-1 | 12/12 | 20:14 | DST/D | 14° 38,062' N | 024° 54,193' W | 2395 | With BGC drifter |
| M160-147-1 | 12/12 | 21:59 | MSN | 14° 36,643' N | 024° 54,846' W | 2662 | Profile depth 1000 m |
| M160-148-1 | 12/12 | 23:21 | CTD/RO 58 | 14° 37,653' N | 024° 54,309' W | 2510 | Profile depth 1200 m |
| M160-149-1 | 13/12 | 01:37 | CTD/RO 59 | 14° 35,978' N | 025° 05,009' W | 4229 | Profile depth 1200 m |
| M160-150-1 | 13/12 | 02:39 | MSS 26 | 14° 36,081' N | 025° 04,863' W | 4229 | |
| M160-151-1 | 13/12 | 04:12 | CTD/RO 60 | 14° 36,967' N | 025° 03,888' W | 4161 | Profile depth 500 m |
| M160-152-1 | 13/12 | 04:33 | WRIDE/D | 14° 36,969' N | 025° 03,868' W | 4164 | |
| M160-153-1 | 13/12 | 12:12 | GLD/D | 14° 39,579' N | 025° 22,802' W | 4399 | |
| M160-154-1 | 13/12 | 12:19 | GLD/D | 14° 39,855' N | 025° 22,610' W | 4396 | |
| M160-155-1 | 13/12 | 14:02 | MDRIFT | 14° 41,824' N | 025° 20,233' W | 4390 | |
| M160-156-1 | 13/12 | 14:02 | MDRIFT | 14° 41,817' N | 025° 20,229' W | 4390 | |
| M160-157-1 | 13/12 | 14:03 | MDRIFT | 14° 41,810' N | 025° 20,225' W | 4390 | |
| M160-158-1 | 13/12 | 15:05 | MDRIFT | 14° 45,003' N | 025° 21,681' W | 4357 | |
| M160-159-1 | 13/12 | 15:05 | MDRIFT | 14° 45,020' N | 025° 21,692' W | 4362 | |
| M160-160-1 | 13/12 | 15:06 | MDRIFT | 14° 45,032' N | 025° 21,699' W | 4359 | |
| M160-161-1 | 13/12 | 15:54 | MDRIFT | 14° 48,268' N | 025° 23,718' W | 4367 | |
| M160-162-1 | 13/12 | 15:54 | MDRIFT | 14° 48,278' N | 025° 23,724' W | 4367 | |
| M160-163-1 | 13/12 | 15:54 | MDRIFT | 14° 48,287' N | 025° 23,731' W | 4367 | |
| M160-164-1 | 13/12 | 21:26 | DST/R | 14° 53,113' N | 024° 53,325' W | 3647 | |
| M160-165-1 | 13/12 | 22:34 | CTD/RO 61 | 14° 54,011' N | 024° 54,311' W | 3731 | Profile depth 1000 m |
| M160-166-1 | 14/12 | 02:58 | CTD/RO 62 | 14° 26,134' N | 025° 14,933' W | 4414 | Profile depth 500 m |
| M160-167-1 | 14/12 | 03:24 | MSS 27 | 14° 26,250' N | 025° 14,807' W | 4412 | |
| M160-168-1 | 14/12 | 04:59 | CTD/RO 63 | 14° 27,504' N | 025° 13,716' W | 4394 | Profile depth 1200 m |
| M160-169-1 | 14/12 | 09:02 | CTD/RO 64 | 14° 45,008' N | 025° 27,062' W | 4404 | Profile depth 1000 m |
| M160-170-1 | 14/12 | 09:35 | DST/D | 14° 45,022' N | 025° 27,091' W | 4408 | With BGC drifter |
| M160-171-1 | 14/12 | 14:59 | DCTD | 14° 42,029' N | 025° 22,610' W | 4391 | CTD for release |
| M160-171-1 | 14/12 | 15:06 | DCTD | 14° 42,059' N | 025° 22,663' W | 4390 | Start dye release |
| M160-172-1 | 14/12 | 15:30 | GLD/D | 14° 42,181' N | 025° 22,872' W | 4393 | |
| M160-173-1 | 14/12 | 15:38 | GLD/D | 14° 42,200' N | 025° 22,963' W | 4388 | |
| M160-171-1 | 14/12 | 16:01 | DCTD | 14° 42,344' N | 025° 23,199' W | 4392 | End dye release |
| M160-174-1 | 15/12 | 00:05 | MSN | 14° 42,701' N | 025° 29,487' W | 4423 | Profile depth 1000 m |
| M160-175-1 | 15/12 | 01:16 | CTD/RO 65 | 14° 42,701' N | 025° 29,487' W | 4420 | Profile depth 1200 m |
| M160-176-1 | 15/12 | 03:08 | MSS 28 | 14° 43,241' N | 025° 29,337' W | 4420 | |
| M160-177-1 | 15/12 | 03:17 | MSC | 14° 43,252' N | 025° 29,341' W | 4417 | Sampling depth 40 m |
| M160-178-1 | 15/12 | 03:29 | MSC | 14° 43,251' N | 025° 29,341' W | 4418 | Sampling depth 40 m |
| M160-179-1 | 15/12 | 03:58 | CTD/RO 66 | 14° 43,270' N | 025° 29,374' W | 4414 | Profile depth 500 m |
| M160-180-1 | 15/12 | 05:54 | CTD/RO 67 | 14° 44,846' N | 025° 35,111' W | 4474 | Profile depth 1200 m |
| M160-181-1 | 15/12 | 07:34 | MSS 29 | 14° 44,650' N | 025° 35,135' W | 4479 | |
| M160-182-1 | 15/12 | 08:48 | DST/R | 14° 40,136' N | 025° 31,882' W | 4443 | |
| M160-183-1 | 16/12 | 04:22 | MSN | 14° 39,538' N | 025° 45,445' W | 4496 | Profile depth 1000 m |
| M160-184-1 | 16/12 | 05:39 | CTD/RO 68 | 14° 39,208' N | 025° 45,734' W | 4497 | Profile depth 1200 m |
| M160-185-1 | 16/12 | 07:14 | MSS 30 | 14° 38,711' N | 025° 46,535' W | 4502 | |
| M160-186-1 | 16/12 | 07:28 | MSC | 14° 38,486' N | 025° 46,799' W | 4507 | Sampling depth 60 m |
| M160-187-1 | 16/12 | 07:40 | MSC | 14° 38,226' N | 025° 47,071' W | 4509 | Sampling depth 60 m |
| M160-188-1 | 16/12 | 08:18 | CTD/RO 69 | 14° 37,874' N | 025° 47,625' W | 4514 | Profile depth 1000 m |
| M160-189-1 | 16/12 | 09:29 | DST/D | 14° 37,512' N | 025° 48,536' W | 4521 | With BGC drifter |
| M160-190-1 | 16/12 | 10:16 | MSN | 14° 37,960' N | 025° 49,039' W | 4522 | Profile depth 1000 m |
| M160-191-1 | 16/12 | 21:13 | MOOR/R | 14° 34,997' N | 025° 01,476' W | 3976 | KPO 1217 |
| M160-192-1 | 16/12 | 23:35 | WGLD/R | 14° 36,969' N | 024° 51,295' W | 3339 | |

| | | | | | | | |
|---|---|---|---|---|---|---|---|
| M160-193-1 | 17/12 | 00:33 | WGLD/R | 14° 34,624' N | 024° 48,991' W | 3921 | |
| M160-194-1 | 17/12 | 04:23 | CTD/RO 70 | 14° 16,186' N | 025° 15,008' W | 4463 | Profile depth 1200 m |
| M160-195-1 | 17/12 | 06:02 | MSS 31 | 14° 18,165' N | 025° 14,243' W | 4455 | |
| M160-196-1 | 17/12 | 06:33 | CTD/RO 71 | 14° 18,382' N | 025° 14,384' W | 4455 | Profile depth 500 m |
| M160-197-1 | 17/12 | 13:53 | DST/R | 14° 25,541' N | 025° 59,068' W | 4591 | |
| M160-198-1 | 17/12 | 15:02 | CTD/RO 72 | 14° 25,887' N | 025° 59,867' W | 4588 | Profile depth 1000 m |
| M160-199-1 | 17/12 | 17:49 | WRIDE/R | 14° 06,474' N | 026° 07,013' W | 4738 | |
| M160-200-1 | 17/12 | 23:24 | CTD/RO 73 | 14° 45,056' N | 025° 55,085' W | 4562 | Profile depth 1200 m |
| M160-202-1 | 18/12 | 16:16 | GLD/R | 14° 39,703' N | 025° 31,446' W | 4445 | |
| M160-203-1 | 18/12 | 16:53 | GLD/R | 14° 39,764' N | 025° 31,321' W | 4447 | |
| M160-204-1 | 18/12 | 17:15 | GLD/R | 14° 40,054' N | 025° 30,834' W | 4442 | |
| M160-205-1 | 18/12 | 17:30 | GLD/R | 14° 40,830' N | 025° 30,674' W | 4430 | |
| M160-206-1 | 18/12 | 18:15 | GLD/R | 14° 40,365' N | 025° 27,688' W | 4425 | |
| M160-207-1 | 18/12 | 20:55 | GLD/R | 14° 22,603' N | 025° 50,608' W | 4612 | |
| M160-208-1 | 18/12 | 21:06 | FLOAT | 14° 22,782' N | 025° 50,654' W | 4609 | Argo Float |
| M160-209-1 | 18/12 | 21:06 | SVP | 14° 22,800' N | 025° 50,657' W | 4608 | |
| M160-210-1 | 19/12 | 02:16 | SVP | 15° 07,874' N | 025° 42,128' W | 4438 | |
| M160-211-1 | 19/12 | 08:18 | SVP | 16° 05,284' N | 025° 30,532' W | 4262 | |
| M160-212-1 | 19/12 | 12:12 | SVP | 16° 44,300' N | 025° 22,843' W | 2952 | |

# 8 Data and Sample Storage and Availability

Detailed information on storage of data and samples is given below in Table 8.1

**Table 8.1** Overview of data availability

| Type | Database | Available | Free Access | Contact (E-Mail) |
|---|---|---|---|---|
| {IFM03,08,13,14,15} glider data (T, S, P, $O_2$, chl-a, turbidity, nitrate, microstructure) | OSIS → PANGAEA | 03/2020 | 12/2021 | gkrahmann@geomar.de |
| {Amadeus, Sebastian, Comet, Dipsy} glider data (T, S, P, $O_2$, chl-a, turbidity, microstructure) | PANGAEA | 06/2020 | 12/2021 | lucas.merckelbach@hzg.de |
| CTD/O2 data | OSIS → PANGAEA | 03/2020 | 12/2021 | mdengler@geomar.de |
| vmADCP data | OSIS → PANGAEA | 02/2020 | 12/2021 | mdengler@geomar.de |
| Mooring data (ADCP velocity, MMP data) | OSIS → PANGAEA | 03/2020 | 12/2021 | mdengler@geomar.de |
| Microstructure data (from gliders and vessel-based profiles) | OSIS → PANGAEA | 06/2020 | 12/2021 | mdengler@geomar.de |
| Quality-controlled biogeochemical sample data (DO, nutrients, DIC/TA) | OSIS → PANGAEA | 03/2020 | 12/2021 | bfiedler@geomar.de |
| (BGC) Argo float data | Coriolis | 12/2019 | 12/2019 | bfiedler@geomar.de |
| Biogeochemical underway measurements ($pCO_2$, DO, fluorescence, gas tension) | OSIS → PANGAEA | 06/2020 | 12/2021 | bfiedler@geomar.de |
| Wave Glider data ($pCO_2$ DO, fluorescence, gas tension, meteorological parameters, ADCP, EK15) | OSIS → PANGAEA | 08/2020 | 12/2021 | bfiedler@geomar.de |
| BGC surface drifter data ($pCO_2$, DO, fluorescence, gas tension) | OSIS → PANGAEA | 08/2020 | 12/2021 | bfiedler@geomar.de |
| Surface drifter (NOAA) | NOAA ERDDAP | 12/2019 | 12/2019 | bfiedler@geomar.de |
| Grazing rate / V9 18S rDNA sequences | GenBank SRA | 12/2020 | 12/2020 | stoeck@rhrk.uni-kl.de |
| CTD profiles made using Multinet | PANGAEA | 09/2020 | 12/2021 | morten.iversen@awi.de |
| Aggregate size and sinking velocity, microbial respiration in aggregates | PANGAEA | 12/2020 | 12/2021 | morten.iversen@awi.de |
| Aggregate composition | PANGAEA | 12/2020 | 12/2021 | morten.iversen@awi.de |
| Zooplankton distribution | PANGAEA | 05/2021 | 12/2021 | morten.iversen@awi.de |
| Biogeochemical analyses of sediment trap material | PANGAEA | 05/2021 | 12/2021 | morten.iversen@awi.de |
| Spectral downwelling irradiance | PANGAEA | 12/2020 | 01/2021 | martin.hieronymi@hzg.de |
| Spectral sky radiance | PANGAEA | 12/2020 | 01/2021 | martin.hieronymi@hzg.de |
| Spectral water-leaving radiance | PANGAEA | 12/2020 | 01/2021 | martin.hieronymi@hzg.de |
| Spectral remote-sensing reflectance | PANGAEA | 12/2020 | 01/2021 | martin.hieronymi@hzg.de |
| CTD data pelagic biogeochemistry: POC/N, lipids & pigments, DOP, dissolved AA, dissolved combined CHO, CDOM, FDOM, particulate lipids & pigments, primary | PANGAEA | 12/2020 | 12/2021 | aengel@geomar.de |

| | | | | |
|---|---|---|---|---|
| production, bacterial biomass production, flow cytometry, TEP, CSP, CLSM | | | | |
| Biogeochemical analysis of aggregates (POC/N, POP, AA, CHO, lipids & pigments, bacterial biomass production, TEP, CSP, CLSM) | PANGAEA | 12/2020 | 12/2021 | aengel@geomar.de |

## 9 Acknowledgements

We greatly appreciate the wonderful working atmosphere as well as the professionalism and seamanship of crew, officers and Captain of R/V METEOR, which made this ambitious and complex expedition a great success. The Chief Scientist further acknowledges the skillfulness, great working spirit and cooperativeness of the scientific party of M160, which can be proud of its achievements.

## 10 References

Alldredge, A.L., Passow, U., and Logan, B.E. (1993). The abundance and significance of a class of large, transparent organic particles in the ocean. Deep Sea Res. 40: 1131–1140.

Bakun, A., D.B. Field, A. Redondo-Rodriguez, S.J. Weeks, 2010. Greenhouse gas, upwelling-favorable winds, and the future of coastal ocean upwelling ecosystems. Global Change Biol. 16: 1213-1228.

Callies, U., R. Carrasco, J. Floeter, J. Horstmann, and M. Quante (2019). Submesoscale dispersion of surface drifters in a coastal sea near offshore wind farms. Ocean Sci. 15: 865-889, doi:10.5194/os-15-865-2019.

Dickson, A. G., Sabine, C. L., & Christian, J. R. (Eds.) (2007). Guide to Best Practices for Ocean $CO_2$ Measurements. PICES Special Publication 3.

Fiedler, B., D. Grundle, F. Schütte, J. Karstensen, C.R. Löscher, H. Hauss, H. Wagner, A. Loginova, R. Kiko, P. Silva, and A. Körtzinger, 2016. Oxygen utilization and downward carbon flux in an oxygen-depleted eddy in the Eastern Tropical North Atlantic. Biogeosciences 13: 5633-5647, doi: 10.5194/bg-13-5633-2016.

Fischer, G., J. Karstensen, O. Romero, K.-H. Baumann, B. Donner, J. Hefter, G. Mollenhauer, M. Iversen, B. Fiedler, I. Monteiro, and A. Körtzinger, 2016. Bathypelagic particle flux signatures from a suboxic eddy in the oligotrophic tropical North Atlantic: production, sedimentation and preservation. Biogeosciences 13: 3203–3223, doi: 10.5194/bg-13-3203-2016.

Fomba, K. W., Muller, K., van Pinxteren, D., Poulain, L., van Pinxteren, M., and Herrmann, H.: Long-term chemical characterization of tropical and marine aerosols at the Cape Verde Atmospheric Observatory (CVAO) from 2007 to 2011(2014). Atmos. Chem. Phys. 14: 8883-8904, 10.5194/acp-14-8883-2014.

Gallager, S.M. (2016). The Continuous Plankton Imaging and Classification Sensor (CPICS): A Sensor for Quantifying Mesoplankton Biodiversity and Community Structure. American Geophysical Union, Ocean Sciences Meeting 2016, abstract# IS52A-07.

Gargas, E. (1975). A manual for phytoplankton primary production studies in the Baltic. The Baltic Marine Biologists. Publication No. 2, The Danish Agency of Environmental Protection, Hørsholm, 1–88.

Grasshoff, K., Kremling, K., and Ehrhardt, M. (1999). Methods of Seawater Analysis. Weinheim, Germany: Wiley-VCH Verlag GmbH.

Gruber, N., 2011. Warming up, turning sour, losing breath: ocean biogeochemistry und global change. Phil. Trans. R. Soc. A 369: 1980-1996.

Gruber, N., Z. Lachkar, H. Frenzel, P. Marchesiello, M. Münnich, J.C. McWilliams, T. Nagai, and G.-K. Plattner, 2011. Eddy-induced reduction of biological production in eastern boundary upwelling systems. Nat. Geosci. 4: doi: 10.1038/NGEO1273.

Grundle, D.S., C.R. Löscher , G. Krahmann, M.A. Altabet, H.W. Bange, J. Karstensen, A. Körtzinger, and B. Fiedler, 2017. Low oxygen eddies in the eastern tropical North Atlantic: Implications for $N_2O$ cycling. Sci. Rep. 7, 4806, doi: 10.1038/s41598-017-04745-y.

Hauss, H., S. Christiansen, F. Schütte, R. Kiko, M. Edvam Lima, E. Rodrigues, J. Karstensen, C.R. Löscher, A. Körtzinger, and B. Fiedler (2016). Dead zone or oasis in the open ocean? Zooplankton distribution and migration in low-oxygen modewater eddies. Biogeosciences 13: 1977-1989, doi: 10.5194/bg-13-1977-2016.

Hieronymi, M. (2016.) Polarized reflectance and transmittance distribution functions of the ocean surface. Optics Express 24: A1045-A1068.

Hieronymi, M. (2019). Spectral band adaptation of ocean color sensors for applicability of the multi-water biogeo-optical algorithm ONNS. Optics express 27: A707-A724.

Hieronymi, M., D. Müller, and R. Doerffer (2017). The OLCI Neural Network Swarm (ONNS): a bio-geo-optical algorithm for open ocean and coastal waters. Front. Mar. Sci. 4: 140.

Iversen, M.H., N. Nowald, H. Ploug, G.A. Jackson, and G. Fischer (2010). High resolution profiles of vertical particulate organic matter export off Cape Blanc, Mauritania: Degradation processes and ballasting effects, Deep-Sea Res. I 57: 771-784.

Karstensen, J., F. Schütte, A. Pietri, G. Krahmann, B. Fiedler, B., Grundle, H. Hauss, A. Körtzinger, C.R. Löscher, P. Testor, N. Viera, and Martin Visbeck (2017). Upwelling and isolation in oxygen-depleted anticyclonic modewater eddies and implications for nitrate cycling. Biogeosciences 14: 2167-2181, doi: 10.5194/bg-2016-34.

Kirchman, D., K'nees, E., and Hodson, R. (1985). Leucine incorporation and its potential as a measure of protein synthesis by bacteria in natural aquatic systems. Appl. Environ. Microbiol., 49: 599–607.

Lachkar, Z., N. Gruber (2012). A comparative study of biological production in eastern boundary upwelling systems using an artificial neural network. Biogeosciences 9: 293-308.

Lachkar, Z., S. Smith, M. Lévy, O. Pauluis (2016). Eddies reduce denitrification and compress habitats in the Arabian Sea. Geophys. Res. Lett. 43: 9148-9156.

Langdon, C. (2001). "etermination of Dissolved Oxygen in Seawater by Winkler Titration Using the Amperometric Technique. IOCCP Report No. 14, ICPO Publication Series No. 134, Version 1.

Löscher, C.R., M.A. Fischer, S.C. Neulinger, B. Fiedler, M. Philippi, F. Schütte, A. Singh, H. Hauss, J. Karstensen, A. Körtzinger, S. Künzel, and R.A. Schmitz (2015). Hidden biosphere in an oxygen-deficient Atlantic open-ocean eddy: future implications of ocean deoxygenation on primary production in the eastern tropical North Atlantic. Biogeosciences 12: 7467-7482, doi: 10.5194/bg-12-7467-2015.

Long, R.A., and Azam, F. (1996). Abundant protein-containing particles in the sea. Aquat. Microb. Ecol. 10: 213–221.

Merckelbach, L., A. Berger, G. Krahmann, M. Dengler, and J.R. Carpenter (2019). A dynamic flight model for Slocum gliders and implications for turbulence microstructure measurements. J. Atmos. Oceanic Technol. 36: 281–296, https://doi.org/10.1175/JTECH-D-18-0168.1

Niiler, P.P., A.S. Sybrandy, K. Bi, P.M. Poulain, and D. Bitterman (1995). Measurements of the water-following capability of holey-sock and TRISTAR drifters, Deep-Sea Res. I: 42, 1951-1964.

Picheral M., et al. (2010). The Underwater Vision Profiler 5: An advanced instrument for high spatial resolution studies of particle size spectra and zooplankton. Limnol. Oceanogr. Methods 8: 462-473.

Ploug, H., and B.B. Jørgensen (1999). A net-jet flow system for mass transfer and microsensor studies of sinking aggregates. Marine Ecology Progress Series 176: 279–290, doi: 10.3354/meps176279.

Ruddick, K. G., K. Voss, A.C. Banks, E. Boss, A. Castagna, R. Frouin, et al., 2019. A Review of Protocols for Fiducial Reference Measurements of Downwelling Irradiance for the Validation of Satellite Remote Sensing Data over Water. Remote Sensing 11: 1742.

Ruddick, K. G., K. Voss, E. Boss, A. Castagna, R. Frouin, A. Gilerson, et al. (2019). A Review of Protocols for Fiducial Reference Measurements of Water-Leaving Radiance for Validation of Satellite Remote Sensing Data over Water. Remote Sensing 11: 2198.

Schütte, F., J. Karstensen, G. Krahmann, H. Hauss, B. Fiedler, P. Brandt, M. Visbeck, and A. Körtzinger, (2016). Characterization of "dead-zone" eddies in the tropical Northeast Atlantic Ocean. Biogeosciences 13: 5865-5881, doi: 10.5194/bg-13-5865-2016.

Smith, D. C. and Azam, F. (1992). A simple, economical method for mea-suring bacterial protein synthesis rates in seawater using 3H-leucine. Mar. Microb. Food Web 6: 107–114.

Steemann Nielsen, E. (1952). The use of radioactive carbon (14C) for measuring organic production in the sea. J. Cons. Perm. Int. Expl. Mer. 18: 117–140.

Vikström, K., Tengberg, A., and Wikner, J. (2019). Improved accuracy of optode-based oxygen consumption measurements by removal of system drift and nonlinear derivation. Limnology and Oceanography Methods 17: 179–189.

## 11 Major Abbreviations

| | |
|---|---|
| ACE | = AntiCyclonic Eddy |
| ACME | = AntiCyclonic Modewater Eddy |
| CE | = Cyclonic Eddy |
| dCCHO | = dissolved Combined Carboydrates |
| CDOM | = Chromophoric Dissolved Organic Matter |
| CPICS | = Continuous Particle Imaging and Classification System |
| CRM | = Certified Reference Material |
| CSP | = Coomassie Stainable Particles |
| CTD/RO | = CTD Rosette |
| CVOO | = Cape Verde Ocean Observatory |
| dAA | = dissolve Amino Acids |
| DIC | = Dissolved Inorganic Carbon |
| DCTD | = Dye Release CTD |
| DOC | = Dissolved Organic Carbon |
| DOM | = Dissolved Organic Matter |
| DOP | = Dissolved Organic Phosphorus, |
| DST/D | = Drifting Sediment Traps Deployment |
| DST/R | = Drifting Sediment Traps Recovery |
| EBUS | = Eastern Boundary Upwelling Systems |
| FDOM | = Fluorenscent Dissolved Organic Matter |
| FLOAT | = Argo Float |
| GLIDER/D | = Glider Deployment |
| GLIDER/R | = Glider Recovery |
| MDRIFT | = Mini Surface Drifter |
| MOOR/D | = Mooring Deployment |
| MOOR/R | = Mooring Recovery |
| MOSES | = Modular Observation Solutions for Earth Systems |
| MSC | = Marine Snow Catcher |
| MSN | = Multiple Opening/Closing Net (Multi Net) |
| MSS | = Micro Structure Sonde |
| MVP | = Moving Vessel Profiler |
| POC | = Particulate Organic Carbon |
| POM | = Particulate Organic Matter |
| REEBUS | = Role of Eddies for the Carbon Pump in Coastal upwelling Areas |
| SD | = Standard Deviation |
| SVP | = Surface Velocity Program Drifter |
| TA | = Total Alkalinity |
| TDN | = Total Dissolved Nitrogen |
| TEP | = Transparent Exopolymeric Particles |
| TIA | = Towed Instrument Array |
| TSG | = Thermosalinograph |
| uCTD | = underway CTD |
| vmADCP | = Vessel-mounted Acoustic Doppler Current Profiler |

| | |
|---|---|
| UVP | = Underwater Vision Profiler |
| WVGL/D | = Wave Glider Deployment |
| WVGL/R | = Wave Glider Recovery |
| WRIDE/D | = Wave Rider Deployment |
| WRIDE/R | = Wave Rider Recovery |